

URMAS JOOST

Impurity and preparation dependent
properties of titania thin films



DISSERTATIONES SCIENTIA MATERIALIS UNIVERSITATIS TARTUENSIS

II

DISSERTATIONES SCIENTIA MATERIALIS UNIVERSITATIS TARTUENSIS

II

URMAS JOOST

Impurity and preparation dependent
properties of titania thin films



UNIVERSITY OF TARTU
PRESS

Institute of Physics, Faculty of Science and Technology, University of Tartu,
Estonia

The Dissertation was admitted on June 19, 2014, in partial fulfilment of the requirements for the degree of Doctor of Philosophy in materials science, and allowed for defence by the Scientific Council on Materials Science of the Faculty of Science and Technology of the University of Tartu.

Supervisor: Dr. Vambola Kisand, Institute of Physics,
University of Tartu

Opponent: Prof. Mika Valden, Optoelectronics Research Centre,
Tampere University of Technology

Commencement: August 26, 2014 at University of Tartu, Tartu, Estonia

This work has been partially supported by graduate school “Functional materials and technologies” receiving funding from the European Social Fund under project 1.2.0401.09-0079 in Estonia.



European Union
European Social Fund



Investing in your future

ISSN 2228-0928
ISBN 978-9949-32-637-2 (print)
ISBN 978-9949-32-638-9 (pdf)

Copyright: Urmas Joost, 2014

University of Tartu Press
www.tyk.ee

CONTENTS

| | |
|--|-----|
| LIST OF PUBLICATIONS..... | 6 |
| ABBREVIATIONS..... | 8 |
| 1 INTRODUCTION..... | 9 |
| 2 LITERATURE OVERVIEW:..... | 11 |
| 2.1 Sol-gel method..... | 11 |
| 2.2 Spin coating..... | 13 |
| 2.3 Photo-induced processes..... | 14 |
| 2.4 Photocatalysis..... | 14 |
| 2.5 Superhydrophilicity..... | 15 |
| 2.6 Band gap engineering..... | 16 |
| 2.7 X-ray photoelectron spectroscopy..... | 18 |
| 3 MATERIALS AND METHODS..... | 23 |
| 3.1 Preparation of the films..... | 23 |
| 3.2 XPS studies..... | 24 |
| 3.3 Characterization of hydrophilic and photo-catalytic properties..... | 25 |
| 3.4 Optical measurements..... | 25 |
| 3.5 Microscopy and surface morphology..... | 25 |
| 4 RESULTS AND DISCUSSION..... | 26 |
| 4.1 Structure of the films..... | 26 |
| 4.2 Changes in chemical composition and elemental distribution during annealing..... | 36 |
| 4.3 Photo-induced processes on the surfaces of the films..... | 41 |
| 4.4 Titania nanoparticle based thin films..... | 47 |
| 5 CONCLUSIONS..... | 53 |
| 6 KOKKUVÕTE..... | 56 |
| ACKNOWLEDGEMENTS..... | 58 |
| REFERENCES..... | 59 |
| PUBLICATIONS..... | 67 |
| CURRICULUM VITAE..... | 151 |

LIST OF PUBLICATIONS

- I. V. Kisand, **U. Joost**, V. Reedo, R. Pärna, T. Tätte, J. Shulga, A. Saar, L. Matisen, A. Kikas, I. Kink, “Influence of the heating temperature on the properties of nickel doped TiO₂ films prepared by sol-gel method”, *Applied Surface Science* 256 (2010) 4538–4542.
- II. R. Pärna, **U. Joost**, E. Nõmmiste, T. Käämbre, A. Kikas, I. Kuusik, M. Hirsimäki, I. Kink, V. Kisand, “Effect of cobalt doping and annealing on properties of titania thin films prepared by sol-gel process”, *Applied Surface Science* 257 (2011) 6897–6907.
- III. R. Pärna, **U. Joost**, E. Nõmmiste, T. Käämbre, A. Kikas, I. Kuusik, M. Hirsimäki, I. Kink, V. Kisand, “Effect of different annealing temperatures and SiO₂/Si(100) substrate on the properties of nickel containing titania thin sol-gel films”, *Physica Status Solidi A* 209 (2012) 953–965.
- IV. **U. Joost**, R. Pärna, M. Lembinen, K. Utt, I. Kink, M. Visnapuu, V. Kisand, “Heat treatment and substrate dependent properties of titania thin films with high copper loading”, *Physica Status Solidi A* 210 (2013) 1201–1212.
- V. **U. Joost**, A. Saarva, M. Visnapuu, E. Nõmmiste, K. Utt, R. Saar, V. Kisand, “Purification of titania nanoparticle thin films: Triviality or a challenge?”, *Ceramics International* 40 (2014) 7125–7132.
- VI. **U. Joost**, K. Juganson, M. Visnapuu, M. Mortimer, A. Kahru, E. Nõmmiste, U. Joost, V. Kisand, A. Ivask, “Antibacterial mechanisms of photocatalytically active anatase nanoparticles based TiO₂ thin films”, *Nanotechnology* (submitted).

AUTHOR'S CONTRIBUTION

As can be seen from the list of publications the present research involves an output of numerous people. The reason lies in the complex nature of the samples, which requires application of various experimental techniques for their characterization and an expertise of a number of scientists. The outcome produced within the frame of the research papers is a group effort. Author's contribution to each research paper is given in the list below.

- I. The Author participated in preparation of the manuscript. The Author is responsible for preparing the samples using sol-gel method, measuring of XPS spectra, AFM images and light-induced hydrophilic properties of the samples.
- II. The Author participated in preparation of the manuscript. The Author is responsible for preparing the samples using sol-gel method, Author participated in the measurement of XPS spectra, measured AFM images, Raman spectra, UV-Vis absorbance and light-induced hydrophilic properties of the samples.
- III. The Author participated in preparation of the manuscript. The Author is responsible for preparing the samples using sol-gel method, Author participated in XPS and XAS measurements, measured AFM images, Raman spectra, UV-Vis absorbance and light-induced hydrophilic properties of the samples.
- IV. The Author is responsible for the manuscript and preparing the samples using sol-gel method. The Author participated in XPS measurements and analysed the data, interpreted Raman spectra, measured UV-Vis absorbance and estimated optical band gaps. The Author also measured hydrophilic properties of the samples and the photocatalytic activity of the samples.
- V. The Author is responsible for the manuscript, synthesising the nanoparticles using sol-gel method and preparation of the films. The Author participated in XPS measurements, analysed XPS data and interpreted Raman spectra.
- VI. The Author is co-responsible for the manuscript (together with K. Jurganson and M. Visnapuu). The Author is responsible for synthesising the nanoparticles using sol-gel method and preparation of the films. The Author also measured and analysed the XPS spectra.

ABBREVIATIONS

| | |
|------------|--|
| AES | Auger electron spectroscopy |
| AFM | Atomic force microscopy |
| AMRSF | Average matrix relative sensitivity factors |
| CFU | Colony forming units |
| DLS | Dynamic light scattering |
| EDX | Energy dispersive X-ray |
| FIB | Focused ion beam |
| FWHM | Full width at half maximum |
| IR | Infrared |
| PES | Photoelectron spectroscopy |
| REELS | Reflection electron energy loss spectroscopy |
| SEM | Scanning electron microscopy |
| UHV | Ultra-high vacuum |
| UV | Ultraviolet |
| UV-A | Ultraviolet A, 315-400 nm |
| UV-B | Ultraviolet B, 280-315 nm |
| UV-Vis | Ultraviolet, visible |
| UV-Vis-NIR | Ultraviolet, visible, near-infrared |
| XAS | X-ray absorption spectroscopy |
| XPS | X-ray photoelectron spectroscopy |
| XRD | X-ray diffraction |

I. INTRODUCTION

Titania (TiO_2) is widely used in industry and our everyday life, it finds use as white pigment and anticaking agent in paints, plastic, paper and other consumer products. It also finds application in sunscreens as UV blocker and foodstuff as coloring agent (E171).

Titania has been considered as a perspective material for many advanced applications. It has been studied extensively as a promising photocatalyst [1], solar cell material [2], biocompatible material [3], material for anti-fogging and self-cleaning coatings [4, 5]. Nanostructure, crystal structure, purity and other qualities, all play important roles in many of titania applications. For example, the efficiency of TiO_2 photocatalytic properties depends besides its crystal structure also on the grain size [6]. Even the adhesion of living cells on titania films (extremely important for medical implants) depends on the nanostructure of the material [3]. The efficiency of a dye sensitized solar cells is as well influenced by the nanostructure of the material, since the grain size of the material directly influences amount of dye adsorbed on titania surface [7]. Titania has three main crystalline phases: anatase, rutile and brookite. Anatase and rutile are tetragonal and brookite is orthorhombic. Although rutile and anatase are from the same crystal system the lattices are quite different, so are the properties. For example, only anatase exhibits remarkable photocatalytic [8] and photo induced superhydrophilic [4] properties.

A number of deposition methods have been used to prepare doped titania films such as sputtering [9], chemical solution deposition [10], pulsed laser deposition [11], and sol-gel method [12]. For practical applications sol-gel method is widely used because it provides numerous advantages over other fabrication techniques. In certain cases important aspects of the film preparation, such as flexibility in introducing a dopant in large concentrations, purity, homogeneity, stoichiometry, possibility to coat large and complex areas and cost-effectiveness can be achieved by sol-gel method [13].

In the present work influence of the type of the impurity element, substrate pretreatment and annealing temperature to the film structure and photo-induced properties was investigated. Also the influence of surface morphology and specific surface area to the photo-induced properties of the films was investigated.

It is important to note that scientific community uses the word “doping” in narrower (semiconductor physics) and wider meaning. In the present work word doping is used in very general sense, *i.e.* as synonym for “introducing impurity element to the system”. Most probably our doped samples after annealing include two kinds of components: (i) the impurity atoms in the TiO_2 crystal lattice, and (ii) separate phases of impurity atom-based compounds.

It is important to know the behaviour of impurities during annealing and formation of the films, the distribution of the impurity elements is crucial in the forming of the photocatalyst films during annealing. The impurity element in the crystalline lattice can change the electronic properties of titania and the band gap can be shrunk [14, 15, 16]. Photocatalytic reactions occur on the surface

and therefore the behaviour of impurity atoms on the surface is especially important. It is possible that photoactive processes are slowed down considerably when the active surface is covered by non-photocatalytically active compounds.

Our general motivation to deal with the present topic lies in the possible future applications of this system as self-cleaning coatings for windows. Such coatings must have both significant photocatalytic and hydrophilic properties. Aim of the present work is to enhance knowledge about effect of annealing temperature, substrate material, influence of different impurity atoms, film morphology and structure to properties of titania thin films using various experimental techniques. Therefore we chose high impurity atom levels for our experiments (concentration of Ni, Co, and Cu were 4.2, 4.2, and 10 atomic percent, respectively). Such a high impurity level allows to investigate precisely the influence of the impurity elements in this complex oxide system with several experimental techniques to confirm or exclude the presence of different compounds, crystal structures, segregation, etc. Also the influence of high specific surface area of the films was investigated by preparing thin films from titania anatase nanoparticles. The ultimate purpose of this work was to contribute into the development of effective and easy to manufacture self-cleaning surface that could be used in outdoor lighting conditions.

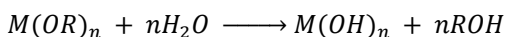
2 LITERATURE OVERVIEW

2.1 Sol-gel method

Sol-gel method enables to produce glasses and ceramics at relatively low temperatures and with relatively low cost. The method is very versatile and enables to prepare a variety of structures e.g. aerogels, xerogels, fibres, nanoparticles and films with precisely controlled parameters of the material e.g. crystallinity, phase composition, grain size and composition.

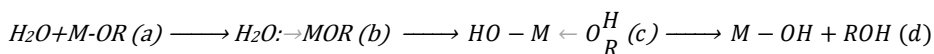
Chemistry of the sol-gel process is based on hydrolysis and condensation of molecular precursors. Mainly there are two different routes depending on whether the precursor is an aqueous solution of an inorganic salt or a metallo-organic compound. The present overview is focused on the second route *i.e.* the hydrolysis and condensation reactions of a metallo-organic precursor ($M(OR)_n$; M refers to metal ion, -OR to the alkoxy group). Electronegative alkoxy groups (-OR) make the metal ion very susceptible to nucleophilic substitution reactions; therefore, it readily reacts with water.

The overall reaction can be written as follows [17]:



The process in detail is complicated and the final oxide network is formed by influence of two chemical processes: hydrolysis and condensation.

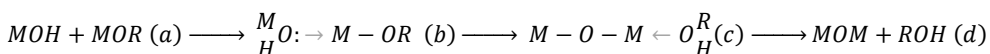
Hydrolysis process can be written in more detail [17]:



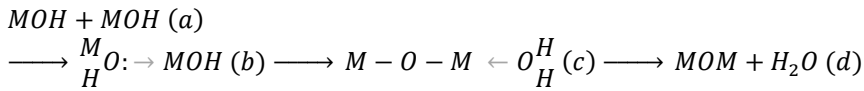
In hydrolysis the first step (a) is a nucleophilic addition of water molecule to the positively charged metal atom M, which leads to the transition state (b) where the coordination number of metal atom has increased by one. The second step involves a proton transfer within (b) leading to the intermediate state (c). A proton from the entering water is transferred to the negatively charged oxygen of an adjacent -OR group. The third step is the departure of the better leaving group (c) leading to metal hydroxide and an alcohol (d). The whole process follows nucleophilic substitution mechanism.

Condensation is a complex process and can occur as soon as hydroxyl groups (-OH) are formed. Depending on experimental conditions three competitive processes have to be considered.

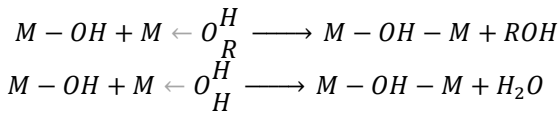
Alkoxolation is a reaction by which a bridging oxo- group is formed through an elimination of an alcohol molecule. The mechanism is basically the same as in hydrolysis with M (metal atom) replacing H in the entering group [17]:



Oxolation follows the same mechanism as alkoxolation, but the R- group of the leaving species is a proton [17]:



Olation can occur when the full coordination of the metal is not satisfied in alkoxide molecule. In this case bridging hydroxo- groups can be formed through the elimination of the solvent molecule. The latter can be either H₂O or ROH (alcohol) depending on the water content in the medium [17].



These four reactions are involved in transfer of the molecular precursors into an oxide network. The resulting structure and morphology of the material strongly depends on the contribution of each reaction. The contributions from each reaction depend on the choice of the alkoxide (type of the metal and alkyl groups) and the reaction conditions (pH, water/alkoxide ratio, temperature, concentration) [17].

In case of titanium alkoxides the initial hydrolysis is fast but the condensation process is slow and the last alkoxide groups are difficult to remove [18, 19]. The condensation starts shortly after the initial hydrolysis step [19]. Hydrolysis and condensation reach metastable state and the reaction can go both ways. The consumption of water at low initial (H₂O/TiO₂<1) water/alkoxide ratio is almost complete. At higher initial water/alkoxide ratios the water is only partially consumed and its consumption tends toward a limiting value and depends upon the complexation ratio of the metal atom. It is also concluded that majority of OH groups are engaged in forming oxo- bridges [20].

In sol-gel process stages involving hydrolysis and condensation reactions are usually conducted in relatively dilute solutions to ensure homogeneity of the processes. Liquid state also simplifies the processing of the material into thin films and coatings. A layer of solid material is formed on a surface after the solvent has been removed. Often highly volatile solvents are used and the drying process is fast. During drying most of the solvent evaporates from the film. When drying takes place in an atmosphere containing water vapour, then hydrolysis and condensation processes continue. Internal stresses appear and may cause the film to crack when drying process is too rapid (cracking process is extensively investigated by J. Jōgi *et al.* [21]).

To form crystalline material the sample has to be annealed. During annealing, changes in the film structure take place: drying, evaporation, oxidation of the organics and crystal phase transitions occur and modify the film structure. As organic residue burns out, the film becomes porous. During further heat treatment the pores collapse and the film becomes denser.

The crystal phase composition of titania is strongly dependent on the choice of preparation method, materials and different parameters used in the process. Sol-gel titania obtained by partial hydrolysis of alkoxides usually yields amorphous material. Crystalline structure is achieved by annealing samples at relatively high temperatures. Anatase crystal phase usually appears after thermal treatment at 400 °C or higher [22, 23, 24]. The phase transition to rutile usually occurs around 800 °C or above [22, 23, 24, 25]. Phase transition temperatures can be influenced by different dopants. For example Mn²⁺ ion concentrations up to 1.5 mol% can stabilize the anatase phase and increase the anatase to rutile conversion temperature, but concentrations over 2 mol% lower the phase transition temperature and accelerate the process [26]. An addition of Si⁴⁺ inhibits the phase transition from anatase to rutile [27, 28]. The change in the phase transition temperature is caused by the formation of an anatase solid solution containing silicon [29] that stabilizes anatase phase. Also Fe³⁺ doping increases the phase transition temperature from anatase to rutile [28]. Even different substrate materials can influence the phase composition of the material and crystal phase transition temperatures [30].

When sol-gel process is slowed down by adding complexing agents or using nonhydrolytic hydroxylation reactions the crystal phase composition can be strongly modified. The addition of diethylamine as complexing agent results in much lower phase transition temperatures for both anatase and rutile i.e. 323 °C and 560 °C, respectively [31]. Sol-gel process can even yield crystalline anatase titania using temperatures as low as 60 °C [32]. Nonhydrolytic sol-gel can be very versatile and yield titania with very high surface area and different crystalline phases (anatase [33, 34, 35], rutile [35] and brookite [35]) depending on the reaction conditions and reagents used.

2.2 Spin coating

Spin coating is a method that enables to cover objects of different shape and size with uniform thin solid films and to control the film thickness with good reproducibility. It is a very robust and reliable method when preparing samples in laboratory scale. Usually a solution of solid material is used as a precursor, the solution is dropped at the centre of a substrate that is spinning or will be spun afterwards. The thickness of the resulting film depends on the viscosity of the solution, the angular speed of the substrate, and the concentration of the solid material in the solution. Mathematical description of the processes occurring during spin coating is relatively difficult. Never-the-less, D. Meyerhofer has proposed an approximation that describes the formation of films during spin coating well enough to provide useful tendencies in the practical application of spin coating method. For example estimating the thickness change of the films when changing the rotation speeds or the concentration of solid material in the solution [36]:

$$h_f = \left(\frac{2}{3}\right)^{\frac{1}{3}} c_0(1 - c_0)^{-\frac{1}{3}} \omega^{-\frac{2}{3}} \nu_0^{\frac{1}{3}} e^{\frac{1}{3}}$$

Where h_f is final film thickness, c_0 is initial concentration of the solid material, ω is the angular speed, ν_0 is the kinematic viscosity of the solution.

Different materials can be used to produce different films e.g. polymer films [37], oxide films [38], nanoparticle films [39] and to create films with different properties and thickness. The thickness of the films can be successfully varied in wide ranges from thin films (>200 nm) to ultra-thin films (<200 nm) [40].

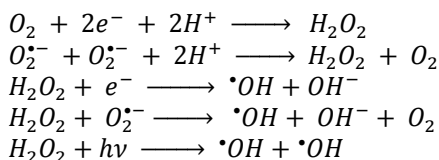
2.3 Photo-induced processes

Photocatalysis and light-induced superhydrophilicity in case of titania are two separate processes which can be activated by the absorption of light. Absorption of a photon with enough energy leads to excitation of an electron from the valence band to the conduction band and creation of a hole in valence band. The photogenerated electron-hole pairs may recombine or drive photo-induced processes. The subsequent mode of action of the generated electron-hole pair will determine which process takes place.

The lifetime of photogenerated electron-hole pairs depends on the structure and electronic properties of the materials, but also the compounds present in the reaction medium can influence photocatalytic reactions. Modification of the materials electronic structure by doping influences the lifetime of electron-hole pairs. The nature and concentration of dopants might play an important role in the lifetime of electron-hole pairs; in some cases the dopant can act as recombination centre and decrease the lifetime of electron-hole pairs [41, 42]. Also, the presence of hole scavengers such as methanol can increase the efficiency of photocatalytic degradation by trapping holes [41, 43].

2.4 Photocatalysis

It has been shown that titania can photo-degrade very different organic compounds [44, 45] [46]. It is assumed that photocatalytic oxidation and reduction reactions occur simultaneously, otherwise charges would build up. Photocatalysis is initiated by electron transfer to oxygen molecule, which is considered also the rate determining step of the reaction. Photogenerated electrons are strong enough reducers to produce $O_2^{\cdot-}$ (superoxide ion). The produced superoxide ion is an effective oxygenation agent and will effectively attack neutral species and surface absorbed radicals. Photoholes will oxidize surface absorbed H_2O , $-OH$ and surface titanol groups ($>TiOH$) into hydroxyl radicals. It is assumed that electron and hole transfer occur simultaneously to maintain charge balance of the process [13]. Also $\cdot OH$ radicals can be generated by other reactions, for example [47]:



On the example of halocarbons it has been shown that the photo-degradation process is initiated by surface adsorbed $\cdot OH$ radicals [48]. There is also evidence that $\cdot OH$ radicals are major species behind photocatalytic degradation of organic compounds and photocatalytic deactivation of microbes. Although other reactive oxygen species also take part of the photocatalytic degradation processes, most of the effect is due to $\cdot OH$ radicals [49, 50] that not only act on TiO_2 surface but can diffuse to the surrounding solution or through small distances in air and effectively degrade organic compounds even not directly in contact with the photocatalyst [49, 51]. Oxidation by $\cdot OH$ radicals might not be the only mechanism of oxidation. It was shown by Tachikawa *et al.* [52] that oxidation efficiency depends on the strength of adsorption of the oxidized molecule to the surface of TiO_2 . R. B. Draper *et al.* [53] conclude that many oxidation reactions on the surface of TiO_2 may occur by direct electron transfer from the organic molecule to TiO_2 .

2.5 Superhydrophilicity

Over time different mechanisms have been proposed to explain why titania has light-induced superhydrophilic properties. The most widespread theory is that Ti^{4+} cations will be reduced to Ti^{3+} by photoelectrons and at the same time photo-holes are trapped at lattice sites (usually bridging oxygen) or close to the surface of the semiconductor. This will weaken the bond between oxygen and titanium allowing oxygen atoms to escape and create oxygen vacancies. Water will dissociatively adsorb on the oxygen vacancies and hydroxylate the surface [13, 54, 55, 56, 57].

It has also been proposed that the change in hydrophilic properties of titania is caused by the photo-oxidation of different contaminants on the surface of titania [58, 59, 60]. Yan *et al.* [58] were not able to fully explain their experimental results concerning photo-oxidation of organic layer and conclude that the mechanism needs further study. Zubkov *et al.* [59] compared the IR spectra of UV irradiated high surface area TiO_2 samples with spectra obtained from non-irradiated samples and found no difference between the spectra. If there had been dissociative adsorption of H_2O on TiO_2 surface as a result of UV irradiation the OH bands in the IR spectra would have changed. J. M. White *et al.* [60] show that there is no difference in water adsorption on stoichiometric and slightly reduced surfaces of TiO_2 indicating that Ti^{3+} has no relation to the light-induced hydrophilic properties of TiO_2 . Light-induced hydrophilic properties cannot be explained only by photo-oxidation of organic contaminant layer on the surface because there are materials that exhibit photocatalytic

properties but do not exhibit light-induced hydrophilic properties and *vice versa* [61]. Nevertheless, the ability to photo-oxidize contaminants on the surface is important to achieve near zero water contact angles, because surface adsorbed contamination layer present on every surface in ambient atmosphere, is usually somewhat hydrophobic.

2.6 Band gap engineering

Photo-induced processes occur when the photon energy of light absorbed in the semiconductor exceeds the band gap of the material. Band gap of TiO₂ anatase and rutile crystalline phase is 3.2 and 3.0 eV, respectively [62, 13]. There are many strategies to inject electrons to the conduction band of titania using light with photon energy smaller than the band gap of the semiconductor material. Dye molecules can be used to photo-sensitize titania [63, 64, 65], and inject electrons from excited state of the molecule to conduction band of the semiconductor. The adsorbed dye is oxidized upon electron injection and degradation of the dye molecule is avoided by the presence of electron donors. Using dye-sensitization different organic compounds can be oxidized but the oxidation potential of the system is limited to the redox potentials of the active species (oxidized dye molecules) [66]. Photo-sensitization of titania can also occur via surface complex formation between an organic compound and the photocatalyst [67, 68]. The corresponding process is very similar to dye-sensitization, but in this case the active molecules are bound to the semiconductor surface.

Band gap of titania can be shrunk and thus visible light can be utilized to drive photo-induced processes. The band gap is effectively shrunk by doping the material with different elements including nonmetals (N, halogens, B, and C) and metals, often transition metals e.g. Fe, Ni, Co, Cu, V, [14] are preferred. Narrowing of optical band gap by doping due to creation of additional electronic states is also suggested by theoretical calculations (Fig. 1). The strategy is to create additional bands in the band gap of the semiconductor material. For example nitrogen impurity creates additional localized states 0.14 eV above the valence band when nitrogen substitutes oxygen and 0.73 eV above valence band when nitrogen is interstitial [69] [15]. NiO modified P25 titania (far-spread commercial titania nanopowder, primary particle mean size 21 nm, anatase/rutile mixture) shows additional absorbance in the visible region and band gap reduction up to 0.8 eV due to the creation of additional states above the valence band of titania [16]. Optical band gap narrowing and absorbance in the visible region has also been observed when titania is doped with Co [70], Fe [71, 72], Cu [72, 73] and other metals.

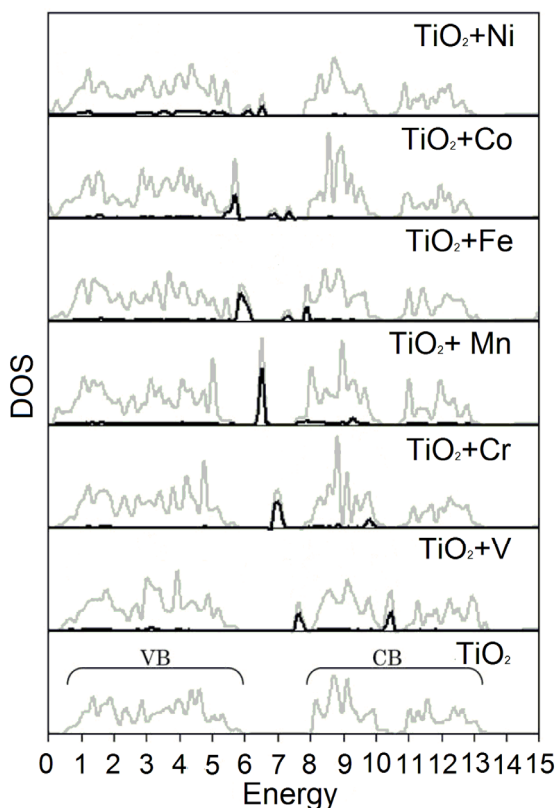


Figure 1. Density of states (DOS) calculated for metal doped rutile TiO_2 , gray solid lines are TiO_2 rutile DOS and black lines represent DOS of the dopant [74].

Visible light can also be utilized to drive photocatalytic reactions by using semiconductor coupling. When a wide band gap semiconductor is coupled with a narrow band gap semiconductor and the narrow band gap semiconductor conduction band level is more negative than the level of wide band gap semiconductor photogenerated conduction band electrons can be transferred from the narrow band gap semiconductor to the wide band gap semiconductor. In order for this kind of a system to work the semiconductors should be photocorrosion resistant, the narrow band gap semiconductor should be able to be excited by visible light and conduction band of the narrow band gap semiconductor should be more negative than the conduction band of the wide band gap semiconductor. The separation of photoelectrons from photoholes also enhances the lifetime of photogenerated electron-hole pairs further improving the efficiency of the photocatalyst system [43]. CdS and CdSe have been successfully coupled with TiO_2 for several applications, for example photo-degradation of 2-chlorophenol [75] and 4-chlorophenol [76] or hydrogen photo-production [77].

2.7 X-ray photoelectron spectroscopy

X-ray photoelectron spectroscopy (XPS) is based on photoelectric effect. When the energy of incident light exceeds the binding energy of an electron, electromagnetic radiation interacts with matter in a way that electrons are emitted. Part of the energy of the radiation is used to free the electron from the nucleus, part of it is used to remove the electron from the material surface and the rest forms the kinetic energy of the electron. Emitted electrons are detected and their kinetic energy is measured to form a spectrum, which contains information about the elemental composition and the chemical bonds in the surface layer of the sample. Electron mean free path is very small [78], thus the probed layer of the sample is extremely thin. The mean free path of electrons is determined by electron-electron and electron-phonon interactions. When dealing with high-energy electrons, electron-phonon interactions lose their relevance and only electron-electron interactions have to be taken into account. The cross-section σ for electron-electron interaction is given as [78]:

$$\frac{d^2\sigma}{d\Omega d\omega} = \hbar \frac{\hbar^2}{(\pi e a_0)^2} \frac{1}{q^2} \text{Im} \left\{ -\frac{1}{\varepsilon(q, \omega)} \right\}$$

where $\hbar q$ is the momentum transfer, ω the energy transfer in the scattering process, $a_0 = 0.529 \text{ \AA}$ (the Bohr radius) and Ω is the solid angle into which the electrons are scattered. From this equation by integration over all energy transfers and momentum transfers the inverse of average mean free path λ^{-1} is obtained. λ^{-1} is essentially determined by the dielectric function [78], which is specific to the material under study and therefore the mean free path is characteristic property of each material. For the energies of interest ($E_{kin} \gg 10 \text{ eV}$), a free-electron gas can approximately describe the electrons since binding energy of valence electrons is in the order of 10 eV. In this case the plasma frequency, which is a function of only the electron density, determines the loss function [78]. The mean electron-electron distance r_s then describes the inverse electron mean free path which is roughly equal for all materials [78]

$$\lambda^{-1} \approx \sqrt{3} \frac{a_0 R}{E_{kin}} r_s^{\frac{3}{2}} \ln \left[\left(\frac{4}{9\pi} \right)^{\frac{2}{3}} \frac{E_{kin}}{R} r_s^2 \right]$$

where $R=13.6 \text{ eV}$, r_s is measured in units of Bohr radius a_0 , and E_{kin} is the kinetic energy of the electron. Since it is experimentally very difficult to measure the mean free path such a relationship is extremely useful in practice, the estimated electron mean free path can be seen on Fig. 2.

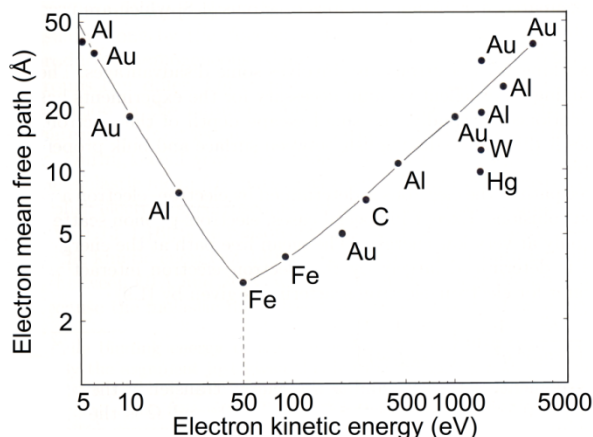


Figure 2. Electron mean free path as a function of kinetic energy for various metals. The data indicate a universal curve with a minimum at 2-5 Å for kinetic energies of 50-100 eV. The scatter of the data is evident from the values obtained at $E_{kin}=1480$ eV [78].

Shifts in the binding energy of an element can occur for different chemical forms of the same atom. This energy difference is called “chemical shift”. Chemical shifts arise due to the differences in screening ability of the electrons of an element in different chemical states. For example in sodium azide (NaN_3) there are two equivalent negatively charged nitrogens N^- and one positively charged nitrogen N^+ . The negative charges (electrons) screen the nuclear charge of nitrogen atom and therefore the binding energy of N^- is smaller than of N^+ , for which screening is absent (Fig. 3). Similar mechanisms are also responsible for chemical shifts in photo-lines of other elements for example C 1s [78]. Chemical shifts can give information about the chemical local bonding environment of the element. Energy of photoelectrons is affected by formal oxidation state of the atom, the identity of its nearest-neighbour atom and bonding hybridization to that nearest-neighbour atom.

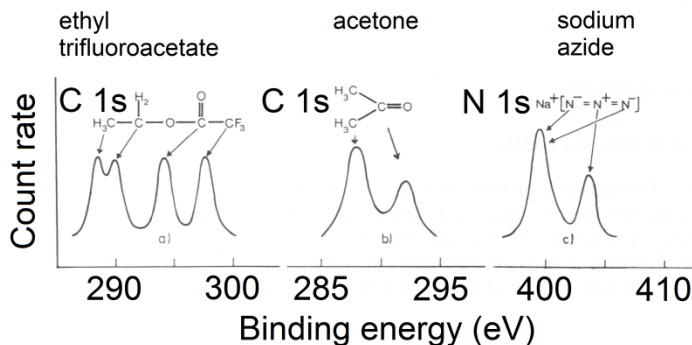


Figure 3. Chemical shifts for the C 1s levels in ethyl trifluoro-acetate, acetone and the N 1s levels in sodium azide [78].

In addition to photoemission lines sometimes so called satellite lines can be observed in the spectrum (Fig. 4). Satellite lines occur when photoemission results in more than one final state. Different screening channels cause satellites in open shell f or d metal ions. The metal ion is assumed to have an unoccupied d level in the initial state. In the photoemission process this empty d level is pulled below the top of the valence band, and formally represents a positive charge on the photoionized ion, generating what is called a two-hole state containing the photohole and the hole provided by the empty state. In metal, it is assumed that the two holes can be screened from the broad sp conduction band, which produces the final state (1). In a different process, charge is transferred from the sp band into the lower d level, thereby producing the second final state (2). Since the localized d level is more efficient in screening than the extended sp band, this second final state has a smaller binding energy than the first one [78].

In insulators the situation is similar. In the initial state the metal ion has an unoccupied d level and an unoccupied broad sp band, which are both pulled down by the core hole to below the top of the ligand valence band. The screening can now occur by charge transfer out of the occupied ligand levels into the metal sp (final-state (1)) band or into the metal d level (final-state (2)), as seen in Fig. 4 [78].

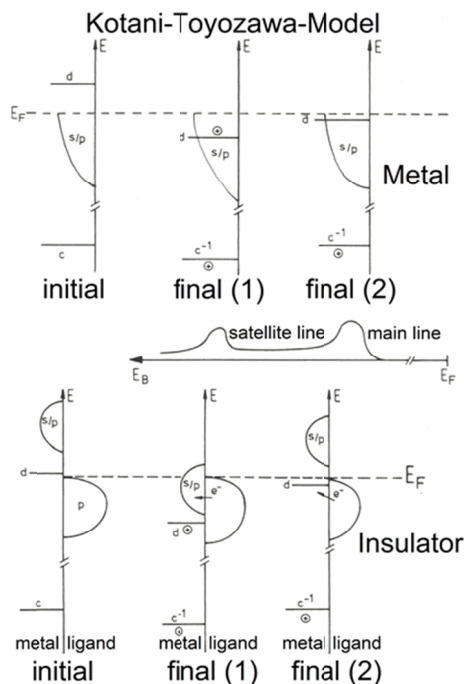


Figure 4. Schematic representation of the Kotani-Toyozawa model for photoelectron spectroscopy (PES) from a core level in a metal and an insulator [78].

In XPS spectra also Auger lines can be present. Auger process occurs when a core electron is removed, and the core hole is filled with an outer shell electron. If the energy difference between the two electron orbitals is transferred to another outer shell electron, it can be ejected and detected. The kinetic energy of the ejected electron does not depend on the excitation energy, but only on the energy difference of the outer shell electron orbital and the core hole to be filled.

One of the most important issues associated with quantitative and chemical analysis using XPS is background correction due to inelastic scattering of electrons. Usually there are three choices: “linear”, “Shirley”, and “Tougaard” background correction methods. Linear approximation of background is the simplest and crudest method, but can be found useful in cases where the background is simple and high accuracy is not needed. Shirley background correction method is very widely used. In Shirley background correction method the background intensity at any given binding energy is proportional to the intensity of the total peak area above the background in the lower binding energy peak range. This approximation is easy to use and the errors are generally not too big. Tougaard method tries to quantitatively describe the physical processes leading to formation of background. S. Hüfner [78] describes and compares Shirley and Tougaard background correction methods. In comparison with the experimental results “Shirley” and “Tougaard” methods perform similarly but differ from the experimental results (REELS) considerably, as can be seen in Fig. 5. Reflection electron energy loss spectroscopy (REELS) is the best method to obtain information about the background in XPS and AES spectroscopy. The main difference between information acquired from REELS and XPS and AES background will come from the fact that REELS electrons will penetrate the surface twice and surface plasmons are enhanced in REELS spectrum [79]. In case of pure samples Tougaard background gives very similar results to REELS data, but Tougaard background correction method could benefit from taking surface excitations into account [80]. The choice of the background correction method is not critical, more important is the consistent use and systematic use of the same background and integration limits throughout one analysis [81, 82].

It has been demonstrated by S. Tougaard [83] that information about the surface structure and chemical composition distribution can be extracted from XPS spectra. Information on the concentration depth profile in the surface region up to 5λ (λ , free mean path) depth is primarily contained in the spectral energy region up to 100 eV (kinetic energy scale) before the photo-line and is essentially completely contained by the energy region up to 200 eV before the photo-line. The method is based on the fact that with every inelastic scattering event electron loses 15-30 eV of energy, and by analyzing the background shape it is possible to deduce the surface structure of the sample.

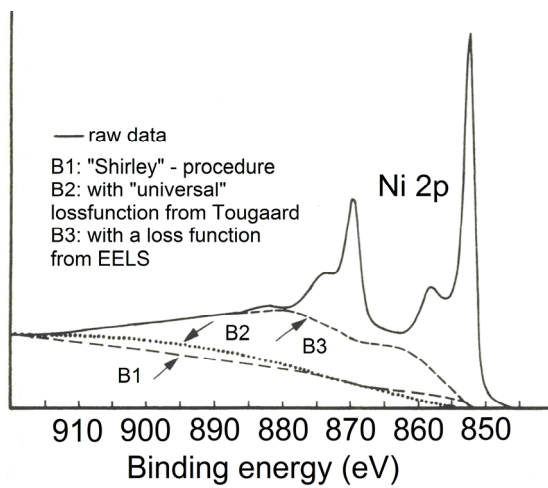


Figure 5. Comparison between Shirley and Tougaard background correction methods [78].

3 MATERIALS AND METHODS

3.1 Preparation of the films

In the present work two different types of thin films were investigated. The thin sol-gel films were prepared by using sol-gel method and spin coating. The films prepared were always uniform and without visible cracks. Commercially available chemicals were used: titanium (IV) n-butoxide (Vertec, purity 98+% or Sigma-Aldrich, reagent grade), nickel chloride hexahydrate (Alfa Aesar, purity 99.95%), cobalt nitrate hexahydrate (Alfa Aesar, purity 99.95%), copper (II) nitrate hemi(pentahydrate) (Sigma-Aldrich, purum), *p*-toluene sulfonic acid (PTSA) (Sigma-Aldrich, reagent plus), acetyl acetone (acac) (Sigma-Aldrich, reagent plus), butanol (Sigma-Aldrich). The chemicals were used as received; only butanol was further purified by distillation over CaH₂ to remove water. The films were prepared on different substrates: silicon monocrystal Si(100), fused silica and soda-lime glass. The impurity elements were introduced as salts of the respective element during the synthesis of the precursor. It was assumed that the impurity elements were distributed homogenously in the precursor material and no contradicting evidences were found during later investigation of the samples. Usually the precursor was dissolved in butanol and the coating parameters were optimized for the process to achieve films with good quality. After preparation the films were stored at ambient conditions for several days to allow the films to dry and the hydrolysis process to occur slowly. After drying the precursor films were annealed at a wide range of temperatures, from room temperature to 1200 °C in air atmosphere to burn off the organic residue and turn the amorphous sol-gel material into crystalline TiO₂. Further details about the preparation of titania thin films can be found in the published works (I, II, III, IV, V).

Besides thin sol-gel films, the present work also investigated nanoparticle based thin films. Namely, using sol-gel method it is possible to synthesize highly crystalline titania anatase nanoparticles at low temperatures in liquid media. The particles are readily dispersible in different solvents for example acetone and lower alcohols, especially in ethanol. Good quality nanoparticle based films can be manufactured using these nanoparticles. Such films were prepared slightly differently than the sol-gel titania films. The synthesis of the nanoparticles is based on the work done by E. Scholan and C. Sanchez [32] but synthesis parameters were slightly modified and optimized to achieve better crystallinity of the material. Extremely small nanoparticles with good anatase structure and narrow size distribution were prepared (see Fig. 6 and 7). The nanoparticles were dispersed in acetone or ethanol and spin coated onto substrates. More details about thin nanoparticle based films are given in work [V].

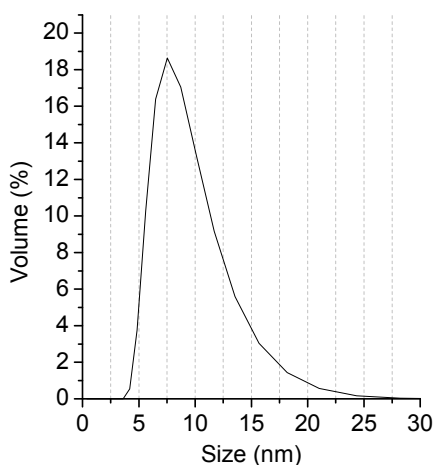


Figure 6. Hydrodynamic size distribution of titania nanoparticles measured with dynamic light scattering [V].

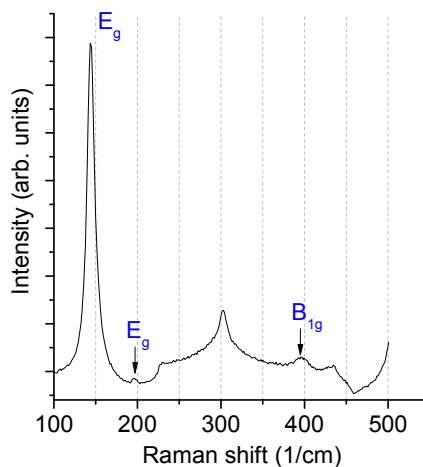


Figure 7. Raman spectra of anatase titania nanoparticles prepared by sol-gel method [V].

3.2 XPS studies

The XPS was carried out in our home laboratory using Scienta SES-100 electron energy analyzer and nonmonochromatized Thermo XR3E2 twin anode X-ray source with characteristic energies of 1253.6 eV (Mg $K_{\alpha 1,2}$ FWHM 0.68 eV) and 1486.6 eV (Al $K_{\alpha 1,2}$ FWHM 0.83 eV). All XPS measurements were conducted in ultra-high vacuum (UHV) conditions. The angle between incoming photon beam and the axis of the electron energy analyzer was 45° and the sample normal was parallel to the axis of the electron energy analyzer.

Measurements employing synchrotron radiation were carried out at beamline D1011 of the MAX II storage ring (Lund, Sweden). Beamline D1011 is equipped with a modified SX-700 plane grating monochromator. For measuring the XPS spectra, an electron energy analyzer (SCIENTA SES-200) in the fixed analyzer transmission (FAT) mode with 200 eV pass energy was used. The binding energy scales for the XPS experiments were referenced to the binding energy of Ti $2p_{3/2}$ (458.6 eV) photoemission line.

To estimate overall atomic concentrations of different compounds and elements average matrix relative sensitivity factors (AMRSF) procedure [84] and our instruments transmission function were used. Raw data was processed using Casa XPS [85] software. Data processing involved removal of K_{α} and K_{β} satellites, removal of background and fitting of components. However, the absolute amounts of different compounds and elements have to be considered cautiously and are given to outline trends only due to the possibility of surface region deviation from chemical homogeneity in the working range of photoelectron spectroscopy (surface region with thickness up to three electron mean free paths).

3.3 Characterization of hydrophilic and photo-catalytic properties

The degree of hydrophilicity was estimated by measuring the contact angle of a water drop on the film, *i.e.* the angle at which the liquid–vapour interface meets the solid–liquid interface. We performed the contact angle measurements using a sessile drop method.

Photocatalytic activity of thin titania films was measured using model contaminants Rhodamine 6G, Brilliant Blue FCF, stearic acid, oleic acid and linoleic acid. Brilliant Blue FCF (absorbance maximum at 628 nm) and Rhodamine 6G (absorbance maximum at 530 nm) were chosen due to their high absorbance coefficients in the visible region that enables to monitor small changes in the amount of dye on the surface of the films. Stearic acid, oleic acid and linoleic acid were chosen to study the mechanisms involved in the decomposition of different fatty acids. In case of Rhodamine 6G and Brilliant Blue FCF the surface was irradiated with a low pressure mercury lamp (maximum at 254 nm) and in case of fatty acids UV lamp with emission in the UV-A range (maximum at 355 nm) was used.

3.4 Optical measurements

Optical transmission and reflection measurements were conducted with a Jasco V-570 (UV/Vis/NIR) spectrometer with specular reflectance accessory.

The crystalline phases of the titania films were examined by measuring room-temperature Raman spectra of the films prepared on a fused-silica substrate using Renishaw micro-Raman setup equipped with 514 nm continuous mode argon ion laser and the spectral resolution was approximately 1.5 cm^{-1} .

Dynamic light scattering (DLS) measurements were performed on Malvern Zetasizer Nano, utilizing He-Ne laser (633 nm). Measurement range is material dependent but the maximal range according to the manufacturer specifications is from 0.3 nm to 5 μm .

3.5 Microscopy and surface morphology

Scanning electron microscope (SEM) images were measured and elemental distributions were determined by using an SEM-FIB instrument (FEI Helios 600) equipped with an energy dispersive x-ray (EDX) detector (Oxford Instruments) and option to use focused ion beam (FIB) for cutting the sample.

Investigations of morphological properties of the samples surfaces were performed with atomic force microscopes (AFM) SMENA-B (NT-MDT) and Veeco AFM. Typically, tapping mode was utilized in order to provide optimal performance.

4 RESULTS AND DISCUSSION

4.1 Structure of the films

Structure of the prepared films was thoroughly investigated using multiple techniques [I, II, III, IV, V]. Before annealing sol-gel films were amorphous and the surface was very smooth as can be observed in Fig. 8(a), 9(a) and 10(a,b). The appearance and evolution of granular structures on the surface of titania thin films coincides very well with the appearance of crystalline structure as can be observed from XRD diffractograms of undoped, nickel and cobalt doped titania thin sol-gel films (Fig. 12, 13 and 14) and Raman spectra of nickel, cobalt and copper doped titania thin sol-gel films (Fig. 15, 16 and 17). Anatase crystal phase usually appeared during heating between 300–450 °C, transition from anatase to rutile crystal phase took place above 700 °C, and exact temperature in both cases depended strongly on doping of the material. The appearance of rutile phase on different annealing temperatures leads us to believe that the impurities influence strongly the structure of titania thin sol-gel films.

The crystallite size of sol-gel thin films grows during annealing and the extent of crystallite growth can be linked to appearance of rutile phase. Note that the mean grain size of undoped titania thin films was smaller than the mean grain size of cobalt doped titania thin films at high annealing temperatures (Fig. 9). In case of cobalt doped titania films the crystal phase transition from anatase to rutile started at 750 °C (Fig. 16) and ended at 950 °C but in undoped titania films the transition started at 100 °C higher temperatures and was not complete even at 1050 °C as can be seen from Fig. 12. In addition to grain size, the content of rutile was higher for cobalt doped titania films compared to undoped titania films at high annealing temperatures, suggesting that crystallites consisting of rutile grow larger than crystallites consisting of anatase at any given annealing temperature.

The impurity metal formed secondary compounds inside the titania matrix during annealing. Raman spectra of all three metal doped titania thin films showed besides anatase (bands at 144 cm^{-1} (E_g), 197 cm^{-1} (E_g), 399 cm^{-1} (B_{1g}), 513 cm^{-1} (A_{1g}), 519 cm^{-1} (B_{1g}), and 639 cm^{-1} (E_g) [86]) and rutile (bands at 143 cm^{-1} (B_{1g}), 447 cm^{-1} (E_g), 612 cm^{-1} (A_{1g}), 826 cm^{-1} (B_{2g}) [87]) the existence of a secondary compounds (Fig. 15, 16 and 17). Raman spectra of nickel doped thin films showed bands linked to NiTiO_3 [88, 89], cobalt doped titania thin films showed bands linked to CoTiO_3 [90]. Titania films with high copper loading showed bands linked to CuO [91]. Nickel and cobalt with TiO_2 tend to form titanates [92, 93, 94]. Usually the secondary compounds appeared during annealing, which indicated the segregation of the impurity element out of the titania matrix. One of the driving forces behind the segregation might be oxidation state differences between the impurity atom and Ti^{4+} , the most common oxidation states are for nickel +2, +3, for cobalt +2, +3 and for copper +1, +2. For example when Ti^{4+} ion is replaced in the lattice by Ni^{2+} ion the charge difference has to be compensated.

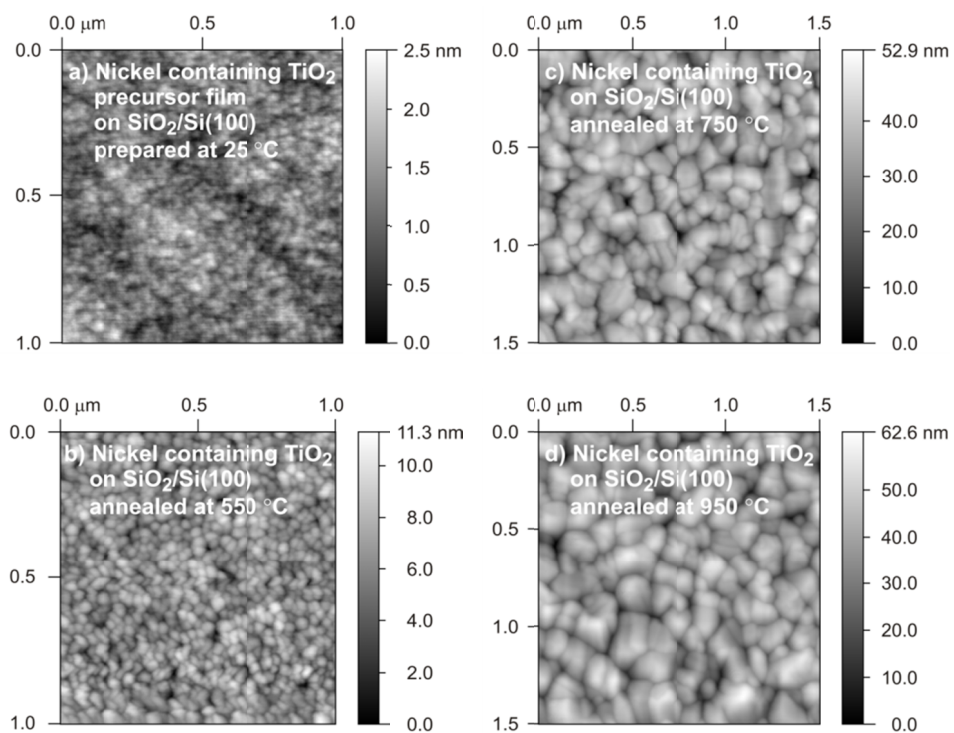


Figure 8. AFM images of a precursor film (a) and nickel containing TiO₂ thin films on SiO₂/Si(100) substrate annealed at 550 °C (b), 750 °C (c) and 950 °C (d). The altitude scale is shown on the right of each image. Note that horizontal scales on the images are different [III].

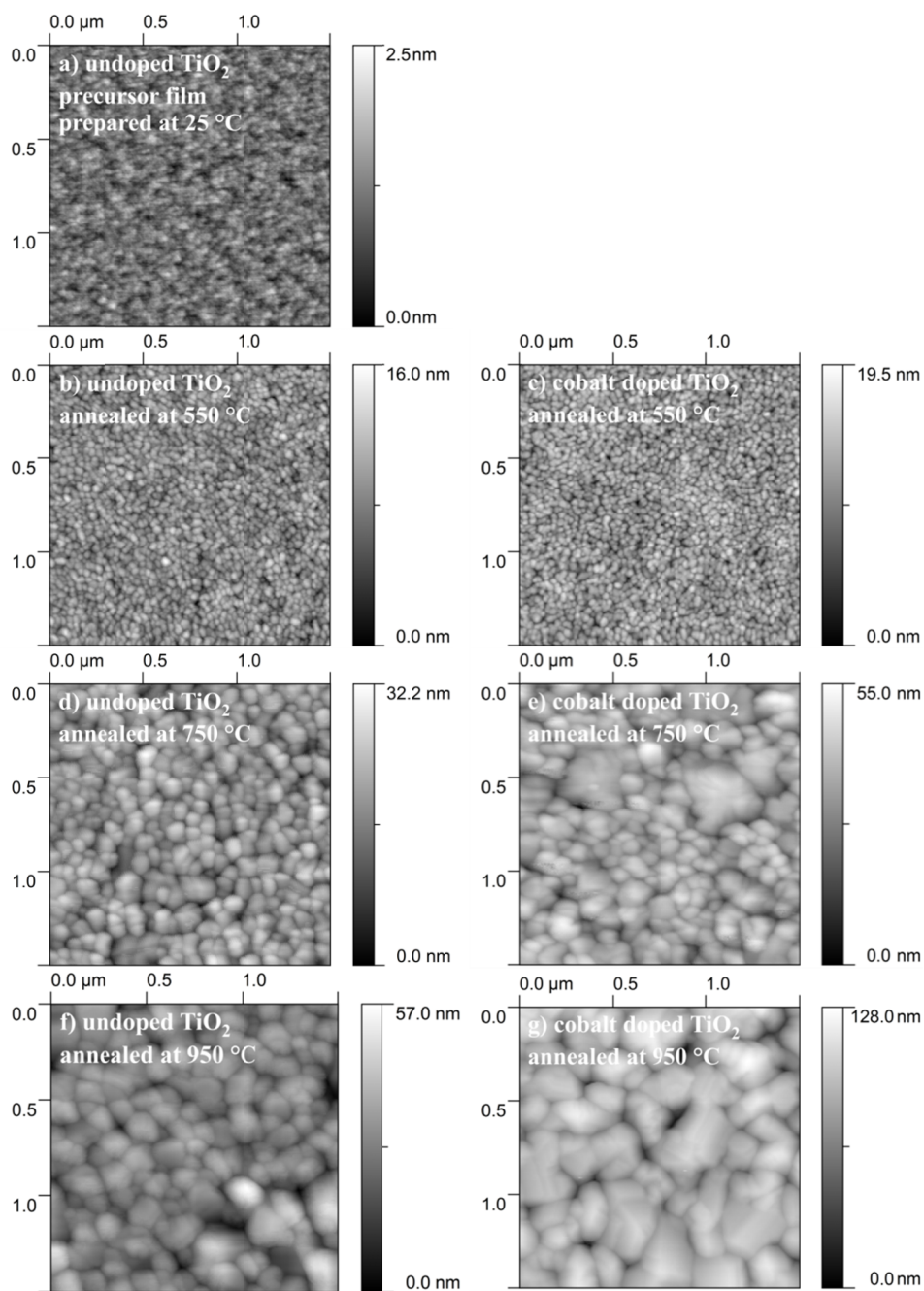


Figure 9. AFM images of undoped TiO_2 precursor film (a) prepared at 25 °C, undoped TiO_2 (b, d, f) and cobalt doped TiO_2 (c, e, g) thin films annealed at 550, 750 and 950 °C. The altitude scale is shown on the right on each image [II].

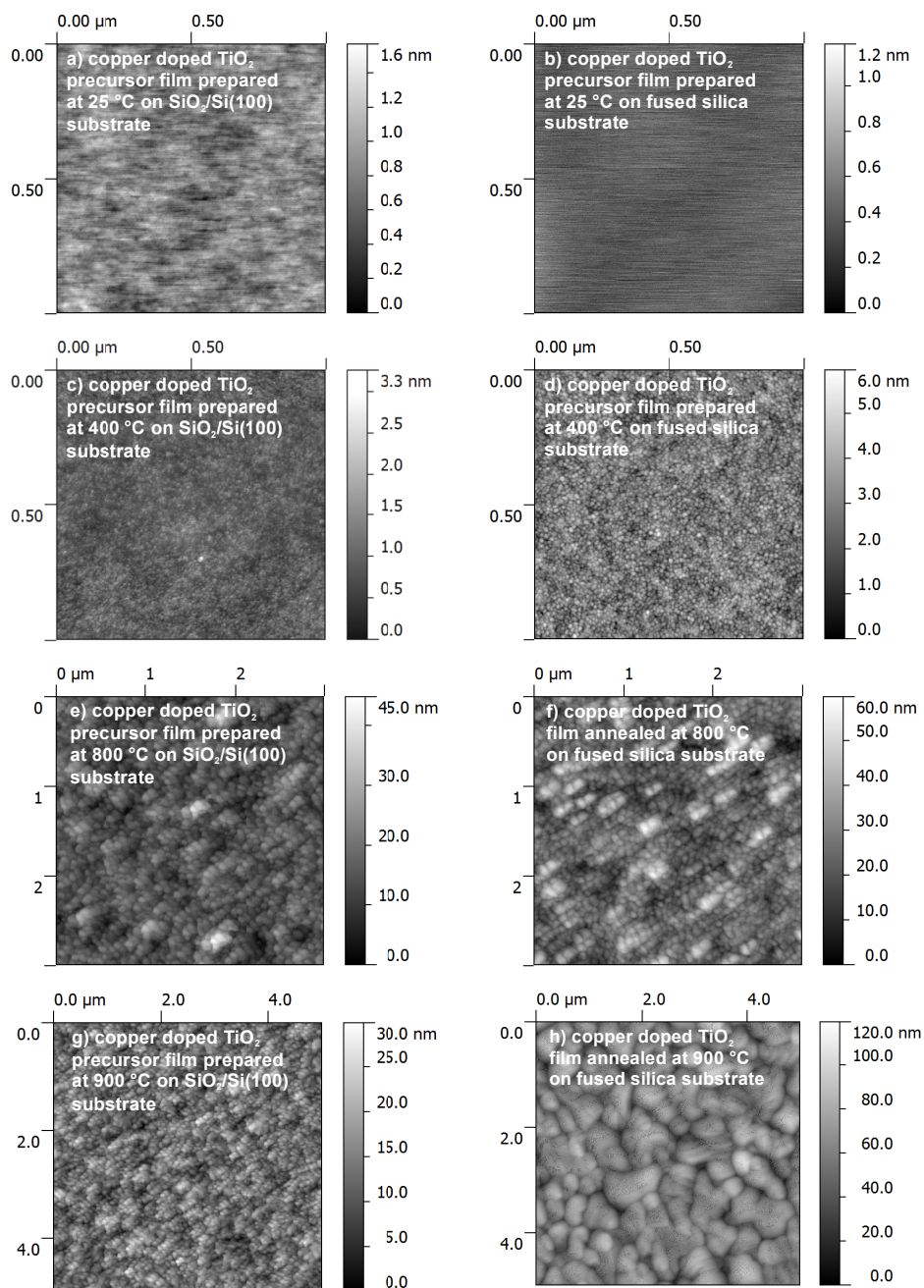


Figure 10. AFM images of copper-doped titania films on $\text{SiO}_2/\text{Si}(100)$ (a, c, e, g) and fused-silica (b, d, f, h) substrates. Precursor film (a, b), films annealed at 400 (c, d), 800 (e, f) and 900 °C (g, h). Films on $\text{SiO}_2/\text{Si}(100)$ substrates are on the left, films on fused-silica substrates are depicted on the right. Note that horizontal scales of the images are different [IV].

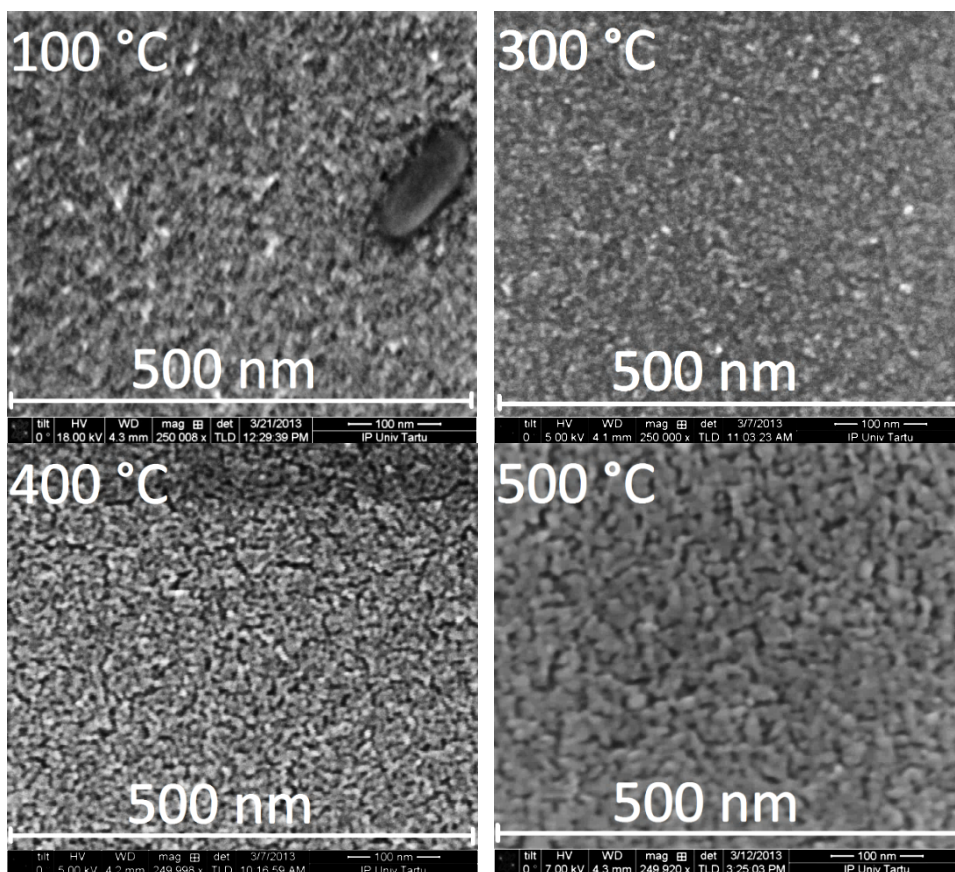


Figure 11. SEM images of 100, 300, 400, 500 °C annealed titania nanoparticle films on SiO₂/Si(100) substrates [V].

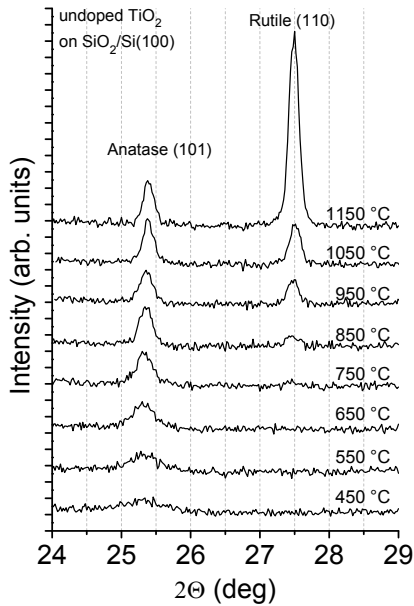


Figure 12. XRD patterns of sol-gel prepared undoped TiO_2 thin films after thermal treatment at different temperatures [II].

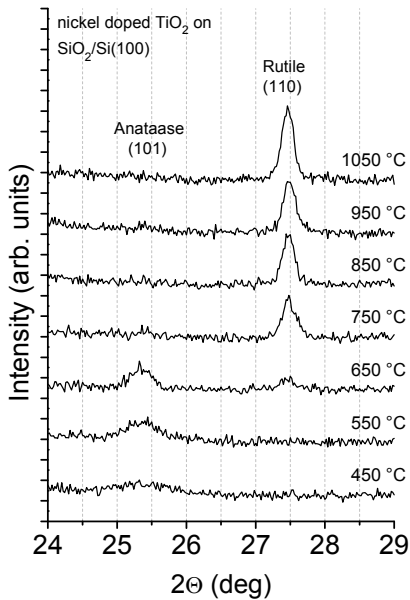


Figure 13. XRD patterns of sol-gel prepared nickel doped TiO_2 samples on $\text{SiO}_2/\text{Si}(100)$ substrate after thermal treatment at different temperatures [III].

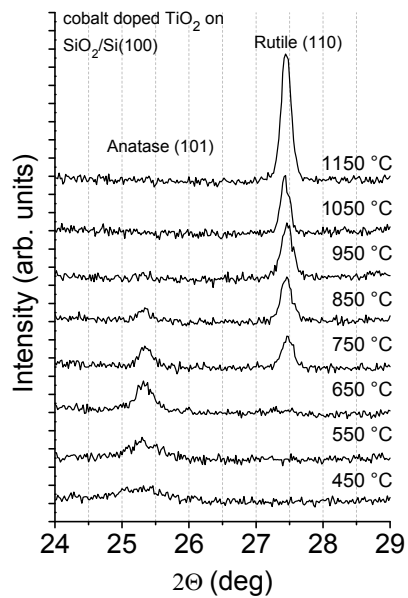


Figure 14. XRD patterns of sol-gel prepared cobalt doped TiO_2 thin films prepared on $\text{SiO}_2/\text{Si}(100)$ substrate after thermal treatment at different temperatures [II].

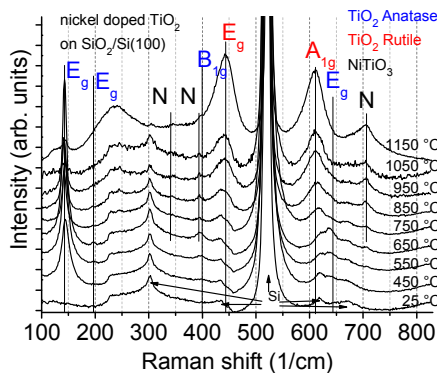


Figure 15. Raman spectra of nickel doped TiO_2 films prepared on $\text{SiO}_2/\text{Si}(100)$ substrate and annealed at different temperatures. Raman spectrum of a precursor film is shown as well (marked as 25 °C). Lines and capital letters demonstrate the positions of TiO_2 anatase (blue), TiO_2 rutile (red) and NiTiO_3 (black) bands. Si substrate bands are shown with arrows [III].

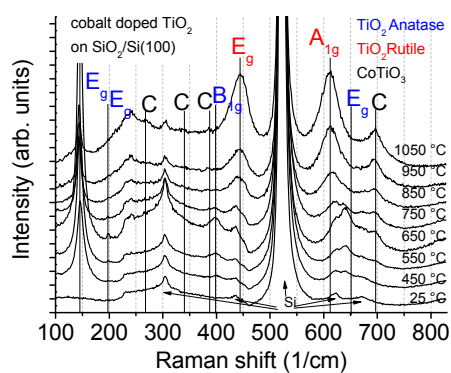


Figure 16. Raman spectra of cobalt doped TiO_2 films prepared on $\text{SiO}_2/\text{Si}(100)$ substrate and annealed at different temperatures. Raman spectrum of precursor film is shown as well (marked as 25 °C). Lines and capital letters demonstrate the positions of TiO_2 anatase (blue), TiO_2 rutile (red) or CoTiO_3 (black) bands. Si substrate bands are shown with arrows [II].

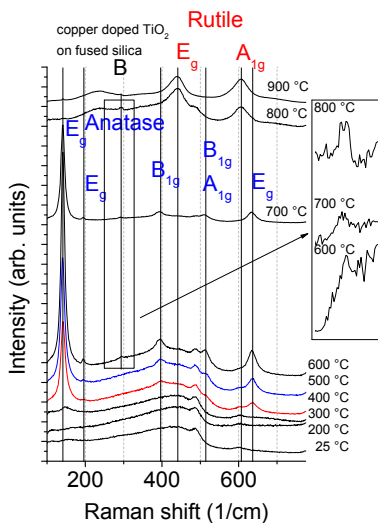


Figure 17. Raman spectra of copper doped TiO_2 films prepared on fused silica substrate and annealed at different temperatures. Vertical lines and capital letters demonstrate the position of TiO_2 anatase (blue), TiO_2 rutile (red) and CuO bands (black) [IV].

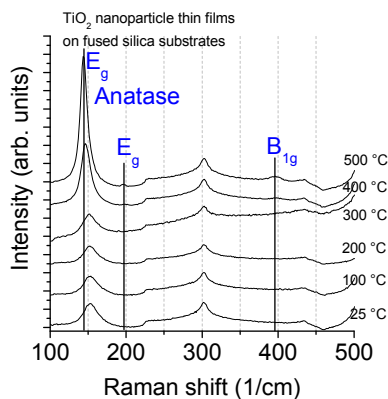


Figure 18. Raman spectra of titania nanoparticle based thin films annealed at different temperatures. Raman spectrum of non-heated film is marked as 25 °C [V].

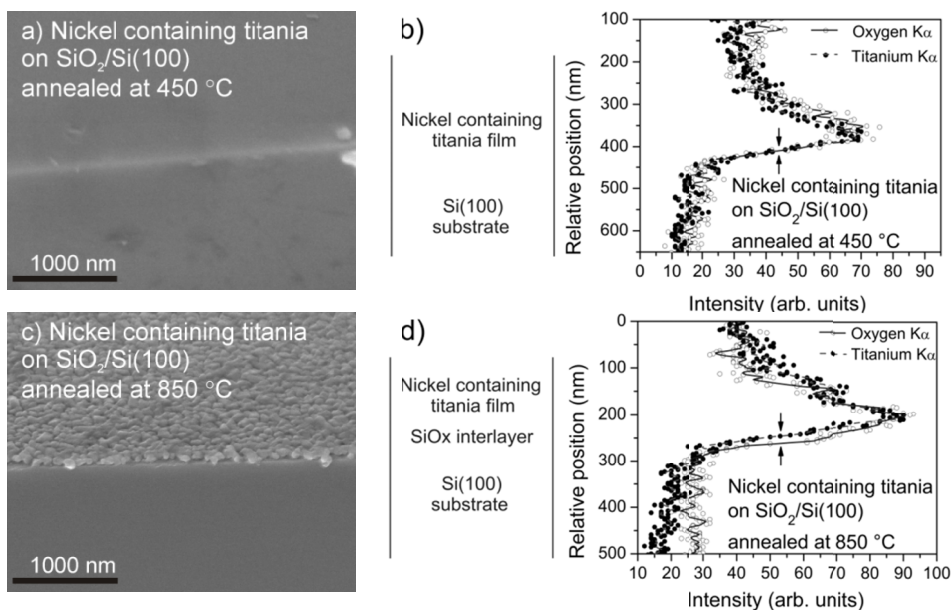


Figure 19. SEM images of nickel doped titania on $\text{SiO}_2/\text{Si}(100)$ substrate annealed at 450 °C (a) and 850 °C (c). EDX spectra of the oxygen and titanium distributions in cross-section of nickel containing titania film on $\text{SiO}_2/\text{Si}(100)$ substrate annealed at 450 (b) and 850 °C (d). On the left side of EDX line scans sketch is shown, which corresponds to cross-section of film. From top to bottom: nickel doped titania layer, SiO_x interlayer (only Fig. 19 d) and the substrate. [III].

The phase transition temperature from anatase to rutile was also influenced by the substrate pre-treatment as can be observed from our work with nickel doped titania thin sol-gel films on $\text{SiO}_2/\text{Si}(100)$ and HF etched $\text{Si}(100)$ substrates [I, III]. In order to detect SiO_2 interlayer or the absence of it between films and substrates we either (i) cut the film, cleaned created cross-section with FIB and measured EDX or (ii) etched rectangular hollow into the films with FIB and measured EDX from the created cross-section. Fig. 19(a) and 19(c) demonstrates cross-sections of cut films imaged with SEM. In EDX experiments we focused on changes between oxygen K_α and titanium K_α radiation as a function of thickness. In Fig. 19(b) and 19(d) oxygen (unfilled dots) and titanium (filled dots) distribution in cross-section of nickel containing titania films on $\text{SiO}_2/\text{Si}(100)$ substrate are demonstrated. Silica interlayers could be observed only for samples annealed at high temperatures (850 and 900 °C, respectively) for both $\text{SiO}_2/\text{Si}(100)$ substrates (Fig. 19) and HF etched $\text{Si}(100)$ substrates. Unfortunately this method is not sensitive enough to detect thin interlayers and native oxide layer on $\text{SiO}_2/\text{Si}(100)$ substrates and films annealed at lower temperatures, so the differences between HF etched and $\text{SiO}_2/\text{Si}(100)$ substrates could not be shown.

During annealing beside changes in the structure of sol-gel films also film thickness decreased remarkably. For example, the precursor film with high copper loading was 250 nm thick and after annealing at 900 °C the thickness of the film decreased to approximately 82 nm *i.e.* more than 3 times (Fig. 20). At lower annealing temperatures film thickness decreased slowly and the decrease can be linked to the decrease of carbon content in the films (Table 1). The sharpest decrease took place during annealing between 500 and 600 °C. This significant decrease of the film thickness is probably related to crystallization of the film. In case of Cu doped thin films intensity of anatase Raman bands increased significantly when annealing temperature was raised from 500 to 600 °C (Fig. 18, red and blue lines, respectively) indicating transformation of amorphous material to anatase. The thickness behaviour during annealing of all sol-gel films with different impurity atoms was principally the same.

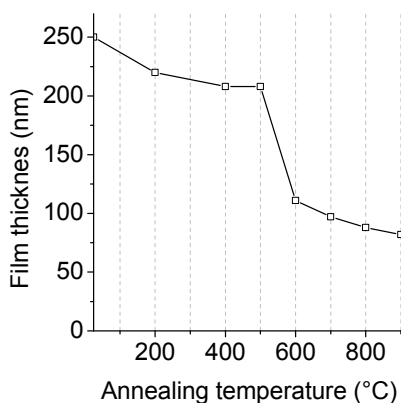


Figure 20. Film thicknesses of copper doped titania thin films evaluated with AFM on SiO₂/Si(100) substrate. Solid lines are eye guides only [IV].

Table 1. Relative concentrations of different compounds and elements (atomic percent) in surface region of copper-doped titania films prepared on SiO₂/Si(100) substrates annealed at different temperatures. Note that compounds undetected by XPS are not taken into account in this table [IV].

| | Copper compounds | | | Ti | C | O | Si |
|--------|-------------------|-----|---------------------|----|----|----|----|
| | Cu ₂ O | CuO | Cu(OH) ₂ | | | | |
| 25 °C | 8 | 0 | 0 | 17 | 20 | 55 | 0 |
| 200 °C | 8 | 0 | 0 | 16 | 25 | 51 | 0 |
| 300 °C | 7 | 2 | 2 | 19 | 15 | 55 | 0 |
| 400 °C | 6 | 17 | 2 | 15 | 12 | 48 | 0 |
| 500 °C | 1 | 18 | 15 | 13 | 10 | 43 | 0 |
| 600 °C | 3 | 16 | 11 | 15 | 8 | 47 | 0 |
| 700 °C | 1 | 10 | 20 | 13 | 6 | 43 | 0 |
| 800 °C | 1 | 1 | 23 | 13 | 7 | 53 | 1 |
| 900 °C | 0 | 0 | 0 | 19 | 7 | 71 | 2 |

Besides sol-gel films, thin TiO₂ nanoparticle based films were prepared [V]. These films had anatase structure from the beginning (Fig. 7) and did not need additional thermal treatment to change amorphous material into crystalline anatase. In this case thermal treatment was only necessary to adhere the films to the substrate and make them mechanically more durable. Films without thermal treatment and films annealed at 100 °C were not durable enough to survive the subsequent washing in ultrasound bath. Films annealed at 200 °C or higher were stable enough to survive washing treatment. The films consisted of small nanoparticles and thus had high specific surface area as can be observed in Fig. 11. Thermal treatment up to 400 °C did not influence the morphology of the films considerably, only slight sintering of the particles was observable. From Fig. 11 it can be seen that the particle size started to increase only after the films were annealed at 500 °C. The same conclusion can be drawn from Raman spectra of titania nanoparticle based thin films (Fig. 18). Raman studies show that the nanoparticle films consisted of anatase. Anatase bands were observed around 144 (E_g), 197 (E_g) and 397 (B_{1g}) cm⁻¹ which correlate well with the literature data [86]. The band originally around 150 cm⁻¹ is shifted at higher annealing temperatures to lower values which are consistent with the work of Li Bassi *et al.* [87] where a shift of 144 cm⁻¹ band to higher values in case of small nanoparticles is shown. From Fig. 16 it can be observed that the band at 150 cm⁻¹ does not start to shift until 400 °C but at 500 °C has already shifted to 144 cm⁻¹ as is reported in literature for bulk anatase [86].

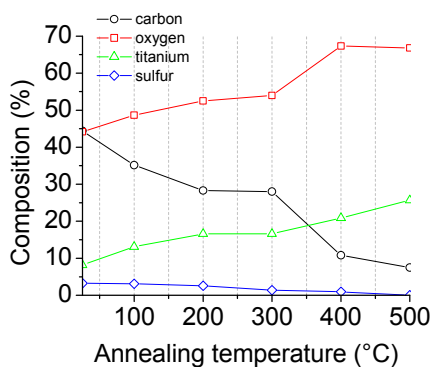


Figure 21. Elemental composition (atomic %) of titania nanoparticle based films annealed at different temperatures from room temperature to 500 °C [V].

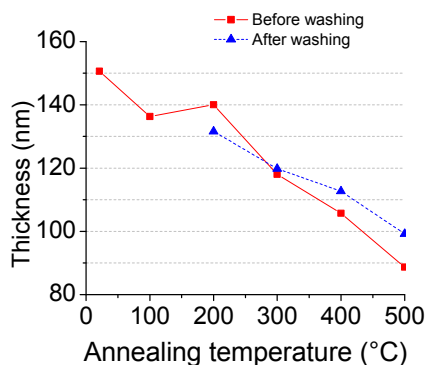


Figure 22. Titania nanoparticles based film thicknesses from AFM measurements after annealing at different temperatures and following washing [V].

Sol-gel based titania thin films required higher annealing temperatures (over 500 °C) to achieve photo-active anatase crystal phase, annealing at high temperatures resulted also in removal of organic material from the sol-gel films.

Titania nanoparticle based films consisted of anatase nanoparticles already before annealing, which makes annealing at high temperatures for crystallization unnecessary. But organic material still needs to be removed and therefore different methods can be applied. One possibility is to anneal the nanoparticle based films in air atmosphere. As can be observed from Fig. 21 annealing is very effective in removal of organic material. The carbon content decreased from 44% to 11% when the nanoparticle based thin films were annealed from room temperature to 400 °C. Annealing to 400 °C did not yet change drastically the morphology and the surface area of the films as was observed by microscopy. During further annealing titania nanoparticle thin films acted similarly to sol-gel films. The thickness of the nanoparticle based films decreased during annealing, but in this case the change in thickness was entirely caused by the removal of organic material from inside region of the films. There was no sharp decrease in the film thickness related to the formation of anatase crystalline phase as could be observed for sol-gel films (Fig. 20 and 22). Destruction of the initial nanostructure of the film can be observed from Fig. 11 for titania nanoparticle thin films annealed at 500 °C. Washing of the films in deionized water and photocatalytic removal of organic material using UV irradiation were also tested for cleaning of samples but the results were not as good, namely, the organic material in the films was replaced with the organic contamination present in the deionised water [V].

4.2 Changes in chemical composition and elemental distribution during annealing

All of the titania thin films showed photoelectron lines of titanium, oxygen, carbon and the added impurity element [I, II, III, IV]. Photoelectron lines of silicon were observable for sol-gel thin films annealed at high temperatures on SiO₂/Si(100) and HF etched Si(100) substrates when the crystallites grew large and narrow gaps between the crystallites were formed. Some of the substrate became exposed giving rise to the Si signal in the spectrum. Sodium and calcium photo-lines were observed due to their diffusion from substrate only when the copper doped titania thin films were prepared on soda-lime glass and annealed at 500 °C (Fig. 23) and above. Sulphur photo-lines were observable in case of titania nanoparticle based thin films [V]. A typical overview spectra of doped titania thin films is shown in Fig. 23.

During annealing the structure of the sol-gel precursor film changed. As well during preparation of precursor once homogeneously distributed impurity elements started to segregate to the surface of the film, resulting in increased concentration of the doping element on the film surface. XPS as surface sensitive technique is extremely suitable for monitoring such changes. This was observed for all three metals investigated in this study as can be observed from Table 1, Fig. 24 and 25. The segregation starting temperature and the extent of

segregation depended of the specific impurity element and the substrate pre-treatment.

Segregation of nickel and cobalt out of titania matrix can also be driven by a second reason, namely formation of NiTiO_3 from NiO and TiO_2 (and CoTiO_3 from CoO and TiO_2) is thermodynamically feasible (standard Gibbs free energy is negative) in the temperature range used in this study [95, 96]. Diffusion of the impurity element in the oxide matrix is limited at low temperatures, so annealing is needed to initiate the process. Segregation process starts when temperatures get high enough to overcome the activation energy needed for the impurity elements to diffuse inside the titania matrix. The appearance of NiTiO_3 (Fig. 15) and CoTiO_3 (Fig. 16) in the samples coincides very well with the segregation of nickel (Fig. 24) and cobalt (Fig. 25) to the surface of the thin films. Out of the three investigated dopants copper behaved slightly differently, copper did not form titanates and was not detected on the surface when copper doped sol-gel thin film were annealed at 900 °C for an hour. The reason behind this was the high vapour pressure of CuO at high temperatures ($9 \cdot 10^{-4}$ mbar ($7 \cdot 10^{-4}$ mm Hg) at 900 °C [97]), enabling the evaporation of copper from the surface layer. However X-ray fluorescence (XRF) analysis (which is more bulk sensitive compared to XPS) demonstrated that copper was still present in the deeper layers of copper doped titania thin films after annealing to 900 °C. Copper concentration of samples annealed at 900 °C dropped to 65% compared to 700 °C (highest surface concentration of copper compounds according to XPS) annealed sample based on XRF analysis.

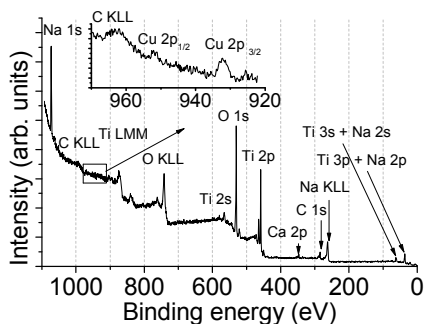


Figure 23. XPS overview spectrum of copper-doped titania film on soda-lime glass substrate annealed at 500 °C for 12 h. Inset on the upper left corner shows XPS spectra of copper 2p lines with smaller scan step [IV].

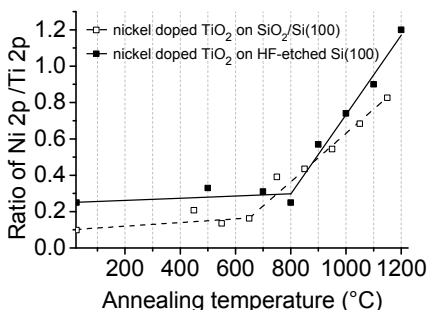


Figure 24. Intensity ratio of Ni 2p and Ti 2p photo lines of nickel doped TiO_2 films on $\text{SiO}_2/\text{Si}(100)$ (dashed line) and HF-etched $\text{Si}(100)$ (solid line) substrate annealed at different temperatures. The respective ratio for a non-heated, aged precursor film is marked as 25 °C is shown as well. The lines are eye guide only [III].

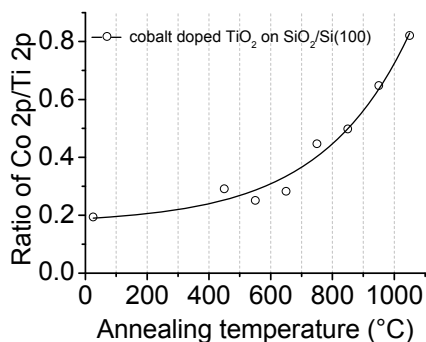


Figure 25. Intensity ratio of the Co 2p and Ti 2p photo-lines of cobalt doped TiO_2 films on $\text{SiO}_2/\text{Si}(100)$ substrate annealed at different temperatures. The corresponding ratio for the non-heated, aged precursor film marked as 25 °C. The solid line is an eye guide only [II].

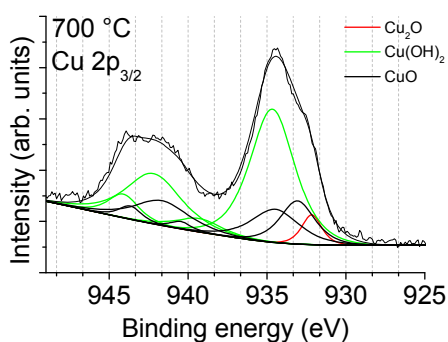


Figure 26. Cu $2p_{3/2}$ photo-line of copper-doped titania thin films on $\text{SiO}_2/\text{Si}(100)$ substrate. At 700 °C annealed copper doped titania film with contributions from Cu_2O (red), $\text{Cu}(\text{OH})_2$ (green) and CuO (black) fitted under the line [IV].

Annealing can change besides the elemental distribution of the impurity metal also the chemical nature of the dopant. It has to be noted that copper was introduced as Cu^{2+} ion into the precursor. In synthesis process of the precursor copper(II) nitrate hemi(pentahydrate) was used as the copper source. During synthesis of the precursor, the solution stayed blue indicating that copper existed in the solution as Cu^{2+} (in case of Cu^{1+} solution should be reddish brown). During drying of the films copper was reduced from Cu^{2+} to Cu^{1+} . Similar reduction of Cu^{2+} to Cu^{1+} was also noticed by Lopez *et al.* [98] and they proposed a mechanism to explain this phenomenon: hydroxide radicals are formed during dehydroxylation of the film and reduce Cu^{2+} to Cu^{1+} .

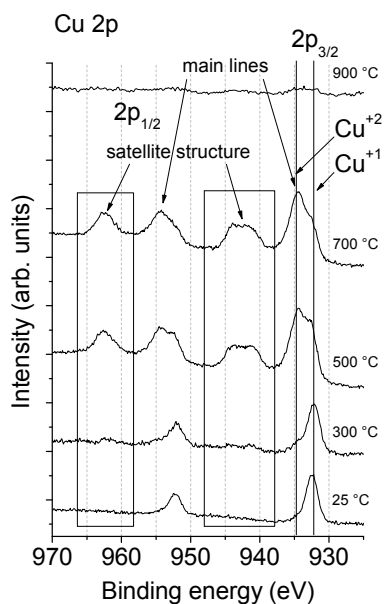


Figure 27. XPS spectra (Cu 2p photo-lines) copper-doped titania thin films on SiO₂/Si(100) substrate. Cu 2p_{3/2} sub-bands typical for Cu¹⁺ and Cu²⁺ are marked as well. Copper-doped TiO₂ films prepared on SiO₂/Si(100) substrate and annealed at 300, 500, 700 and 900 °C. Spectrum of respective non-heated, aged precursor film (marked as 25 °C) is shown as well. Copper 2p signal drops off at 900 °C completely due to evaporation of copper oxide from the surface of the film [IV].

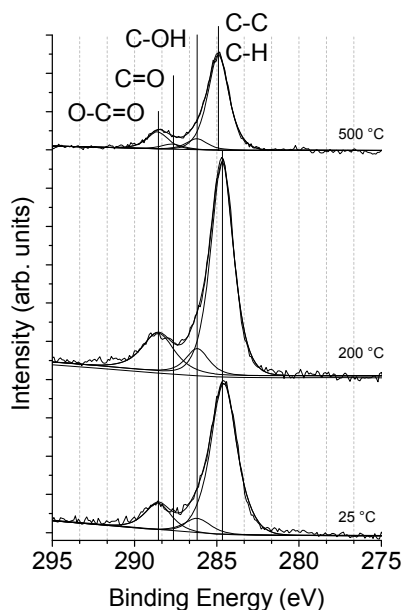


Figure 28. Photoelectron spectra of C 1s region of copper-doped titania thin films on SiO₂/Si(100) substrate of the precursor film (marked as 25 °C) and after thermal treatment at 200 and 500 °C. Sub-bands connected with different carbon compounds are fitted under the experimental spectra [IV].

Fig. 27 displays the Cu 2p photoelectron spectra of the copper doped titania thin films. The observed photoelectron lines are typical for Cu¹⁺ and Cu²⁺ compounds [99]. It can be seen that during annealing Cu¹⁺ is oxidised to Cu²⁺. Cu 2p_{3/2} photo-lines shift to higher binding energy and the appearance of a satellite structure is evidence of presence of Cu²⁺ compounds [100], e.g. as CuO or Cu(OH)₂. Deconvolution of Cu 2p_{3/2} photoelectron spectrum measured from copper-doped titania film on SiO₂/Si(100) substrate annealed at 700 °C is demonstrated in Fig. 26. From the deconvoluted spectra it can be observed that copper exists in three different oxides/hydroxides [101] among which Cu²⁺ exists as two different chemical compounds CuO and Cu(OH)₂. In principle, besides Cu₂O, CuO and Cu(OH)₂ copper carbonate (CuCO₃) might form in the sample, since copper carbonates are formed very often during corrosion of copper surfaces in ambient atmosphere. However in case of copper doped titania films under study, the presence of copper carbonate can be excluded,

since C 1s spectra (Fig. 28) show no signs of CO_3^{2-} at the higher binding energy side of C 1s spectra (289.1–289.6 eV) [102, 103]. CuO appeared in samples annealed at 300 °C or higher temperatures. With the appearance of CuO also $\text{Cu}(\text{OH})_2$ appeared, but it is unlikely that $\text{Cu}(\text{OH})_2$ forms during annealing, since the decomposition temperature of $\text{Cu}(\text{OH})_2$ is 185 °C [104]. It is feasible to conclude that $\text{Cu}(\text{OH})_2$ formed during storage of the copper doped titania thin sol-gel films in ambient atmosphere and the amount of the transformation from CuO to $\text{Cu}(\text{OH})_2$ depends on the exact surface structure and morphology of the films. Transformation from CuO to $\text{Cu}(\text{OH})_2$ is accelerated in case of samples annealed at and above 500 °C and $\text{Cu}(\text{OH})_2$ starts to dominate in samples annealed at and above 700 °C.

If XPS offers possibility to investigate surface region then EDX enables to monitor lateral changes in chemical composition of the samples. Segregation of the impurity element in the titania matrix was observed in sol-gel thin titania films for all three investigated impurity elements. Nickel, cobalt and copper rich regions seem to consist of slightly larger crystallites than undoped samples and appeared on EDX mapping images as light areas (Fig. 29, 30, and 31). Also silicon can be observed in the gaps between the crystallites in the EDX image maps of films annealed at high temperatures.

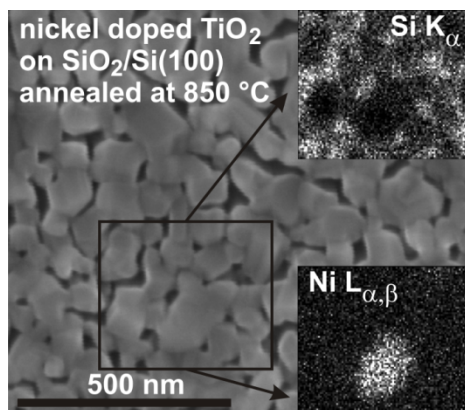


Figure 29. SEM and EDX image (the full image and the insets, respectively) of nickel doped TiO_2 films prepared on $\text{SiO}_2/\text{Si}(100)$ substrates annealed at 850 °C. EDX images of $\text{Ni L}_{\alpha,\beta}$ and Si K_{α} are measured from the area inside the black rectangles and are presented as black and white insets [III].

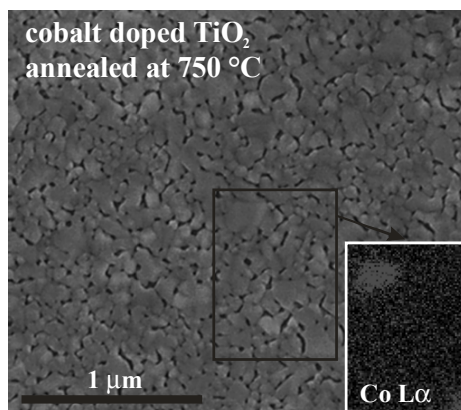


Figure 30. SEM and EDX image (the full image and the inset, respectively) of cobalt doped TiO_2 films prepared on $\text{SiO}_2/\text{Si}(100)$ substrates annealed at 750 °C. EDX image of $\text{Co L}_{\alpha,\beta}$ is measured from the area inside the black rectangles and is presented as black and white inset [II].

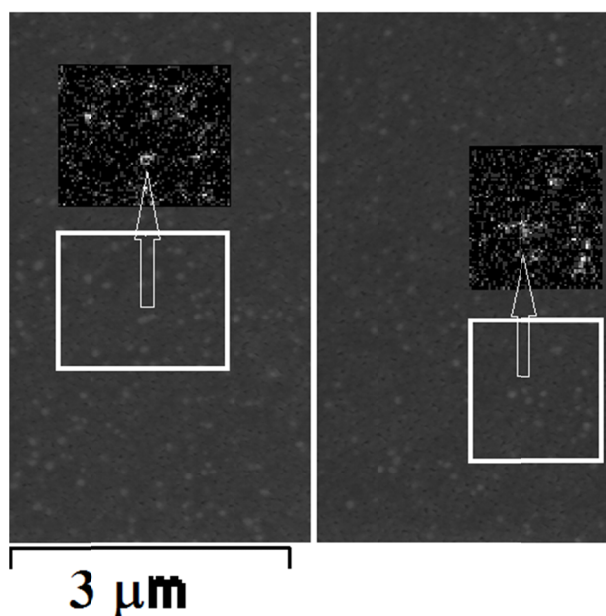


Figure 31. SEM and EDX image (the full image and the insets, respectively) of copper doped TiO_2 films prepared on $\text{SiO}_2/\text{Si}(100)$ substrates and annealed at $700\text{ }^\circ\text{C}$. EDX images of $\text{Cu L}_{\alpha,\beta}$ are measured from the area inside the white rectangles and are presented as black and white inset [IV].

4.3 Photo-induced processes on the surfaces of the films

In order to drive the photo-induced processes semiconductor material has to be illuminated and electron-hole pairs have to be created. Band gap of anatase and rutile is 3.2 eV and 3.0 eV , respectively [62, 13]. Photocatalytically more active anatase has wider band gap, which corresponds to photon energy in the UV region. The Sun has only limited light intensity in the UV region and a fraction of it reaches the sea level on Earth as can be seen from Fig. 32. In case of anatase photo-induced processes can be driven only by UV-light with wavelength less than 385 nm , which makes the useful properties of titania very difficult to apply in real-life applications. In order to increase the efficiency of photo-induced processes of titania, it is necessary to modify the electronic structure of the material (primarily to shrink the band gap while retaining the properties of TiO_2 important for the particular application).

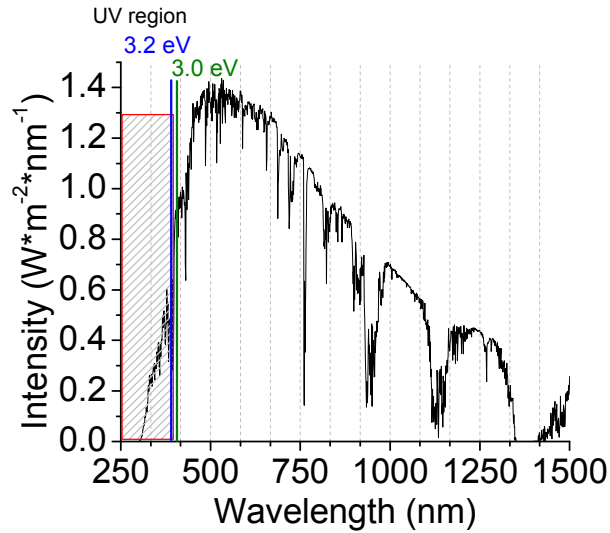


Figure 32. Solar irradiance spectrum on sea level, the data origins from the ASTM G-173 table [105].

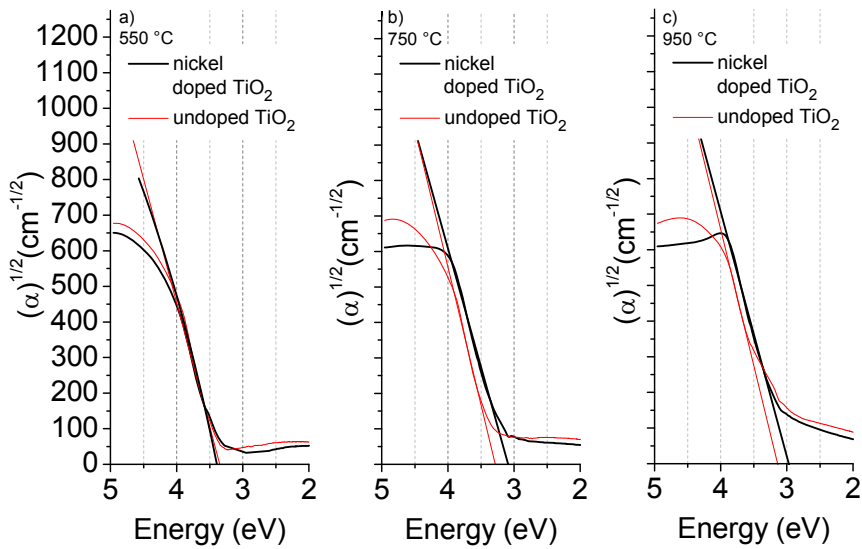


Figure 33. UV-Vis absorption spectra of the nickel doped TiO_2 and undoped TiO_2 reference films annealed at 550 °C (a), 750 °C (b) and 950 °C (c). The spectra are plotted as $\alpha^{1/2}$ versus photon energy graphs [III].

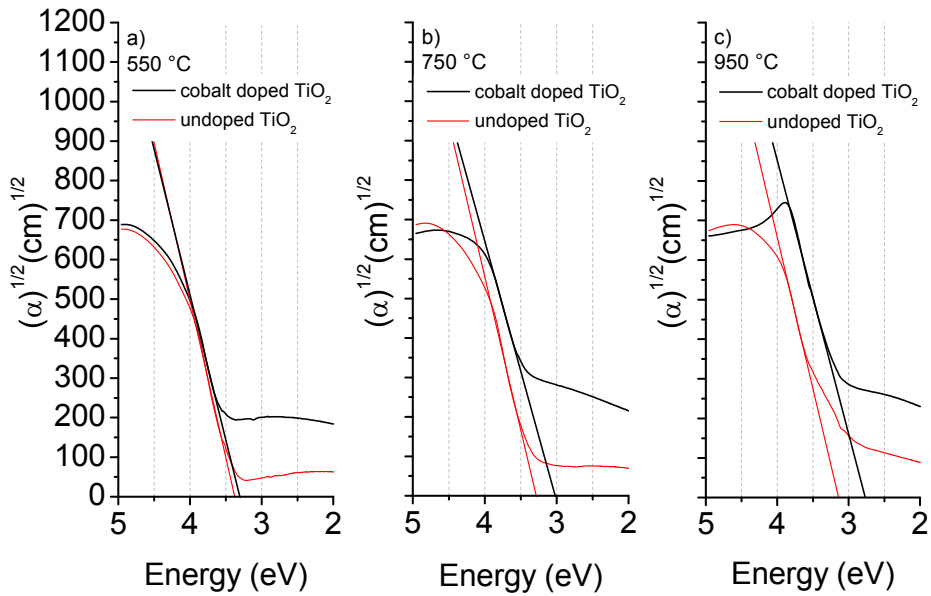


Figure 34. UV-Vis absorption spectra of the undoped TiO₂ and the cobalt doped TiO₂ films annealed at 550, 750 and 950 °C. The spectra are plotted as $\alpha^{1/2}$ versus photon energy graphs [II].

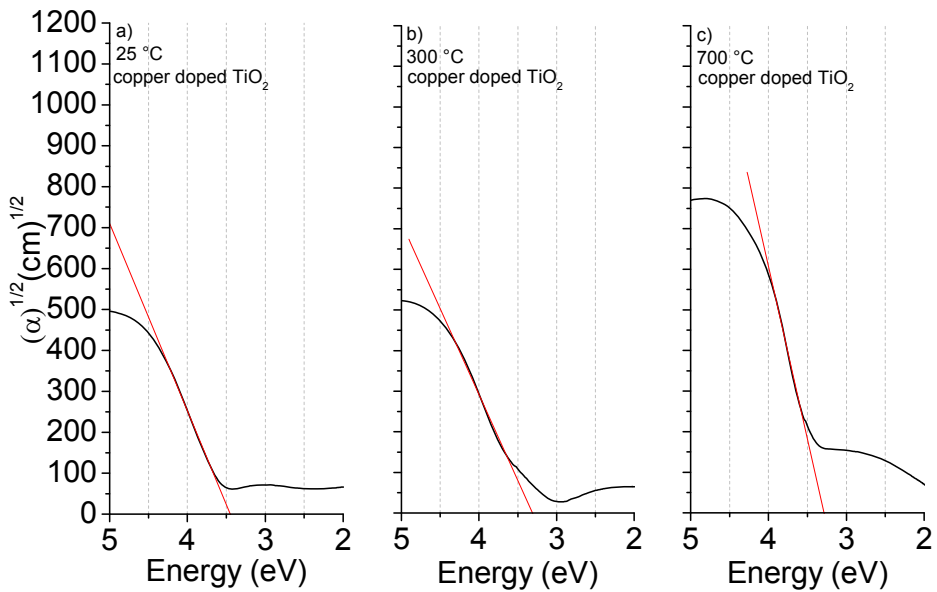


Figure 35. UV-Vis absorption spectra of the copper-doped TiO₂ films precursor film (a) and films annealed at 300 (b) and 700 (c) °C. The spectra are plotted as $\alpha^{1/2}$ versus photon energy graphs [IV].

To evaluate optical properties of doped and pristine titania films UV–Vis transmittance and reflectance measurements were carried out on films prepared on fused-silica substrates [II, III, IV]. The optical absorption coefficients α (Fig. 33-35) were calculated [106] from the measured transmittance (T) and reflectivity (R) by using the evaluated thickness of film (d). From this data the estimation for optical band gap width was deduced. The optical absorption edge of sol-gel titania thin films was shifted to lower energies by addition of nickel (Fig. 33) and cobalt (Fig. 34) relative to the pristine titania thin sol-gel films. Copper did not change the position of adsorption edge but created additional absorption in the visible region of the spectrum, as can be observed from Fig. 35. The shifts in the absorbance edge and additional absorbance in the visible region is probably due to the creation of additional electronic states by the impurity atom in the electronic structure of titania. The influence of secondary compounds and phase shift from anatase to rutile can influence the optical properties of the films and cannot be neglected. For example the band gap of NiTiO_3 , CoTiO_3 and CuO are 2.18, 2.25 and 1.7 eV [107, 108], respectively and will also contribute to the absorbance of doped titania thin films in the visible region.

The surface is called superhydrophilic when a water droplet placed on the surface takes an irregular shape and the contact angle between the droplet and the surface is close to zero degrees. Fig. 36 and 37 demonstrate change of the contact angle as a function of UV-illumination time for Ni and Co doped and undoped TiO_2 samples prepared on $\text{SiO}_2/\text{Si}(100)$ and annealed at different temperatures. As can be seen by comparing Fig. 36 and Fig. 37 undoped titania achieved near zero contact angles sooner than nickel doped titania. Actually, nickel doping did not enhance UV-light induced hydrophilic properties of titania thin sol-gel films, nevertheless nickel doped titania thin sol-gel films on HF etched $\text{Si}(100)$ substrates were able to achieve near zero contact angles when irradiated with an UV diode (photon energy 3.35 eV) mimicking the UV part of the solar irradiance spectrum as can be observed from Fig. 38. Addition of cobalt totally inactivated the light-induced hydrophilic properties of titania thin sol-gel films as can be observed from Fig. 37.

The inhibition of light-induced hydrophilic properties on nickel and cobalt doped titania thin sol-gel films might be due to the blocking of titania surface by nickel and cobalt rich compounds. Also the behaviour of impurity elements in the lattice of titania or secondary compounds in the titania matrix as recombination centres for electron-hole pairs cannot be ruled out and can contribute to the decreased light-induced hydrophilic properties of nickel and cobalt doped titania films compared to the undoped films.

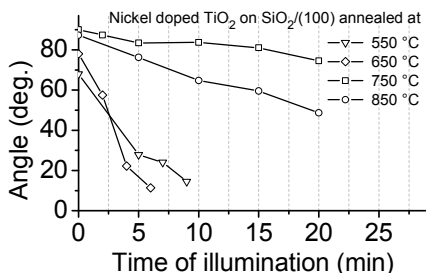


Figure 36. Change of the contact angle as a function of UV-illumination time for the nickel doped TiO_2 samples prepared on $\text{SiO}_2/\text{Si}(100)$ and annealed at different temperatures. Each point represents the duration of UV-illumination before one water droplet was placed on the surface and the contact angle was measured. The illumination source was a Hg-lamp (dominating photon energy 4.89 eV). Solid lines are eye guides only [III].

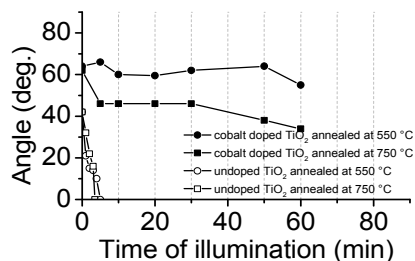


Figure 37. Change of the contact angle as a function of UV-illumination time for the cobalt doped and undoped samples prepared on $\text{SiO}_2/\text{Si}(100)$ and annealed at different temperatures. Each point represents duration of UV-illumination before one water droplet was placed on the surface and contact angle was measured. The illumination source was a Hg-lamp (dominating photon energy 4.89 eV). Solid lines are eye guides only [II].

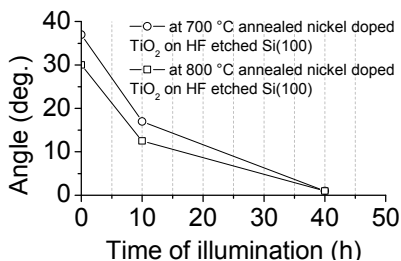


Figure 38. Change of the contact angle as a function of UV-illumination time for the nickel doped samples annealed at 700 °C and 800 °C. UV diode (photon energy 3.35 eV) was used to illuminate the surface [I].

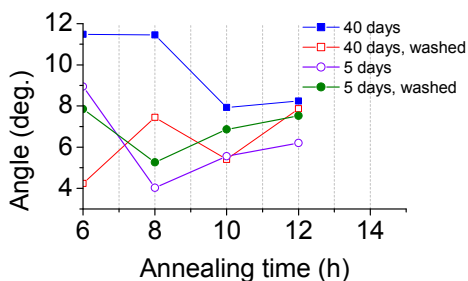


Figure 39. Water droplet contact angles measured on copper-doped titania films prepared on soda-lime glass and annealed at 500 °C for 6–12 h. Contact angles were measured without additional UV exposure (*i.e.* natural hydrophilicity), 5 and 40 days after annealing of the films [IV]

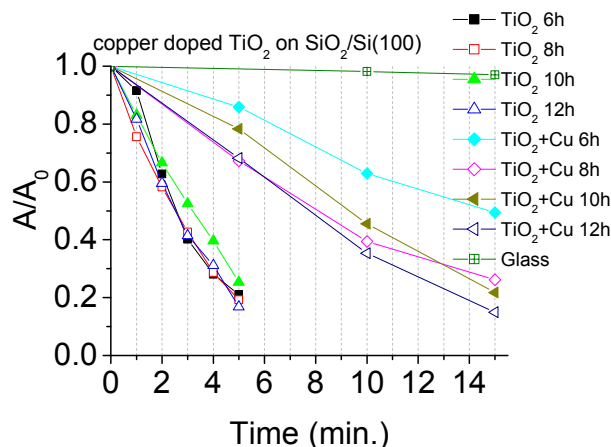


Figure 40. Photo-degradation of model contaminant Brilliant blue FCF on copper doped and pure titania films prepared on soda-lime glass and annealed at 500 °C for 6–12 h and control sample prepared on uncoated soda-lime glass. Photo-degradation is presented as absorption of the dye exposed to UV-light normalized to the dye absorption before exposure [IV].

Additional experiments were conducted to investigate and compare photocatalytic activity of copper doped titania thin sol-gel films to undoped titania films. For technical reasons (film preparation, and UV-Vis measurements) the films were prepared on relatively large and optically transparent soda-lime glass substrates. Films were irradiated with UV-light (dominating photon energy 4.89 eV) in controlled conditions (humidity, temperature). The results (Fig. 40) indicate that photocatalytic degradation of organic material was inhibited by copper doping. Low photocatalytic activity of copper-doped titania films can be explained by several reasons. According to Xin *et al.* [109] excessive oxygen vacancies and Cu compounds at high concentrations can become recombination centres of photo-induced electrons and holes. It would be advantageous to compare photocatalytic activity of our films on different substrates but unfortunately we were not able to measure photocatalytic activity of our films on fused-silica and SiO₂/Si(100) substrates due to restrictions of our setup.

Natural hydrophilicity is a material's property to exhibit small contact angles between the water droplet and the surface without UV-irradiation. Contrary to thin sol-gel titania films doped with either nickel, cobalt or copper prepared on SiO₂/Si(100) or HF washed Si(100) substrates washed with HF, copper doped titania thin sol-gel films prepared on soda-lime glass substrates exhibited naturally hydrophilic surfaces. No irradiation with light was needed to achieve low contact angles (Fig. 39). Measurements of copper doped thin sol-gel films prepared on soda-lime substrates were conducted 5 and 40 days after annealing to ensure time stability of the effect. The films were kept in normal laboratory conditions in the dark and were not irradiated with UV-light prior to measurement. Measurements were conducted twice. The first measurement was

conducted on a film as it was and the second measurement was performed after washing the film with distilled water and drying it in air to eliminate effects caused by different air humidity on different measurement days. Contact angles of copper doped titania thin sol-gel films on fused silica substrate were also measured but the contact angles did not reach low values. Differences in natural hydrophilicity of copper doped titania films on different substrates might be due to different structure and composition of the films. Permpon *et al.* [110] have shown that mixed $\text{SiO}_2/\text{TiO}_2$ films are naturally hydrophilic due to surface acidity. Surface acidity creates OH groups on the surface through dissociative adsorption of water molecules. To achieve high surface acidity a mixed phase has to be present. According to Tanabe *et al.* [111] surface acidity of binary oxides is caused by excessive charges on the doping atom that form because negative atom in the lattice retains its coordination number when bonding to the impurity atom. Charge imbalance might also be one of the reasons why copper segregates out as a separate phase when films are prepared on $\text{SiO}_2/\text{Si}(100)$ silica substrates. When sodium diffuses into the film and destroys the crystal structure of anatase, copper solubility increases and an acidic surface can be formed.

It is important to note that sodium diffusion from the soda-lime glass substrate to the film was observed (see Fig. 23). In case of nickel, cobalt and copper-doped titania films on $\text{SiO}_2/\text{Si}(100)$ substrates or $\text{Si}(100)$ substrates washed with HF, XPS data shows that different dopant rich compounds segregate to the surface (Fig. 24, 25, Table 1), *i.e.* phase separation is in process and mixed phases do not form. Segregation can also be observed from Fig. 29–31 where EDX image maps of nickel, cobalt and copper doped titania films on $\text{SiO}_2/\text{Si}(100)$ substrates show formation of dopant rich regions. For similarly prepared films on soda-lime glass substrates no diffusion of copper oxides to the surface occurs as can be seen from XPS measurements [IV] explaining the difference in surface properties of the films. Unfortunately EDX images of copper doped titania films on soda-lime glass could not be obtained due to heavy charging effects.

4.4 Titania nanoparticle based thin films

In previous chapters the influence of annealing temperature, nature of the impurity atoms, the substrate type and pre-treatment to the properties of sol-gel thin film samples were investigated. In contrast, most of the parameters of the nanoparticles based thin films are determined by the synthesized nanoparticles before thin film preparation and annealing [V, VI]. The crystalline structure and surface morphology are determined by the synthesis of titania nanoparticles (nanoparticle size and crystalline phase). With nanoparticle based systems extremely high specific surface areas of the films can be achieved. Sol-gel thin films need to be annealed to high temperatures to achieve photoactive anatase phase, but at high temperatures the grain size increases to several tens of

nanometres (Fig. 8-10), making it impossible to achieve similar morphology and crystalline structure as nanoparticle based thin films.

Nanoparticles with anatase crystal structure can be synthesized with diameters less than 10 nm (Fig. 6, 7) using wet chemistry methods. The particles are easily dispersible in wide range of solvents in high concentrations (concentrations more than 10% in weight are achievable) and the dispersions are very stable and show no signs of agglomeration and precipitation in the timescale of one year.

Experiments with the nanoparticle based thin films were carried out to evaluate the photocatalytic and bactericidal activity of the films and were conducted in humidity and temperature controlled environment to ensure the repeatability of the experiments [VI]. Realistic values were chosen for the temperature, humidity and UV-A light intensity to estimate the performance of the titania nanoparticle thin films in “real world” applications. Intensity of the irradiation was measured to be ca. 22 W/m^2 in the UV-A region and less than 0.1 W/m^2 in the UV-B region at the surface of the sample. According to ASTM G-173 table [105] UV-A irradiation intensity on the sea level on earth is ca. $30 \text{ W} \cdot \text{m}^{-2}$ and total integrated irradiance for the direct sunlight (used in this work) is taken to be $900.1 \text{ W} \cdot \text{m}^{-2}$. Titania nanoparticle based thin films showed good photocatalytic activity in the UV-A range, as can be observed from decomposition of fatty acids on the surface after UV-illumination (Fig. 42 and 43).

Three different fatty acids – stearic (C18:0), oleic (C18:1 cis-9) and linoleic acid (C18:2 cis-9,12) – were chosen to study the photo-oxidation processes on nanoparticle based titania thin films (Fig. 41). Changes in chemical structure of these acids, the most abundant fatty acids in bacterial cell membranes [112, 113], induced by UV-illuminated titania nanoparticle based thin films were analysed by X-ray photoelectron spectroscopy. The experiment was performed by coating above-mentioned fatty acids on titania nanoparticle based thin films and irradiating with UV-light. XPS spectra obtained from the fatty acids before treatment corresponded well to their structure and the number of carbon atoms in each different chemical state (see Fig. 42). C 1s XPS band components from sp^2 carbon (two single bonds and one double bond) at $284.1 \pm 0.1 \text{ eV}$ [114], sp^3 carbon (four single bonds) at $284.8 \pm 0.1 \text{ eV}$ [115] and carboxylic group (marked as O-C=O) at $288.2 \pm 0.1 \text{ eV}$ [114, 102, 116] could be identified. In oleic and linoleic acid C 1s spectra contributions from both, sp^3 and sp^2 carbons as well as from carboxylic group could be detected (see division of C 1s experimental spectra into the sub-bands); in stearic acid the contributions from sp^3 carbon and carboxylic group could be identified (Fig. 42, 0 minutes irradiation time). In case of stearic acid C 1s spectra, position of the contribution from the carboxylic group is at slightly higher energy at $288.6 \pm 0.1 \text{ eV}$ (Fig. 42 (a)). In the C 1s spectra of stearic and oleic acid the intensity of the contribution from carboxylic group is suppressed due to the tendency of fatty acids to form oriented monolayers [117, 118] where the hydrocarbon chain is located perpendicular to substrate plane, carboxylic group is located on the substrate and the length of molecule is comparable to the escape depth of photoelectrons [119].

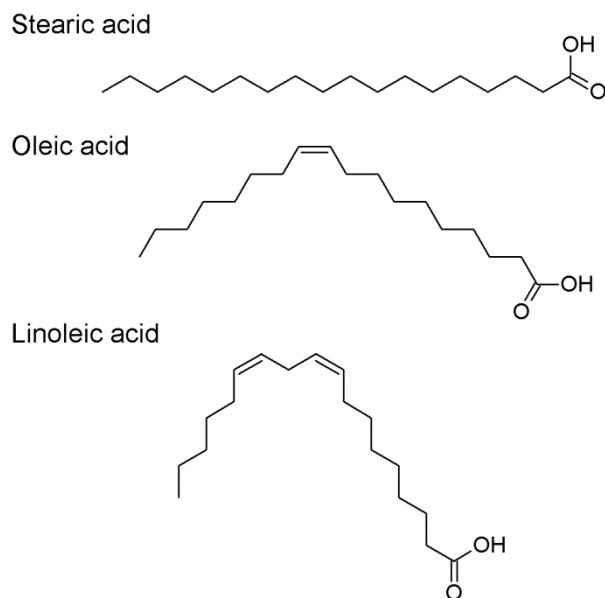


Figure 41. Chemical structure of stearic (C18:0), oleic (C18:1 cis-9) and linoleic acid (C18:2 cis-9,12).

As XPS measurements of photo-oxidized fatty acids were conducted in ultra-high vacuum (pressure in the order of 10^{-10} mbar), photo-oxidation products with low molecular mass and molecules that were not absorbed on the titania surface were removed leaving behind fatty acids directly linked to the surface of nano-TiO₂ films. The latter enabled the monitoring of chemical changes that occurred to fatty acids without the interference from other photo-oxidation products.

XPS spectra of the fatty acids after their exposure to UV-illumination on nano-TiO₂ films (Fig. 42) suggested that photo-oxidation of unsaturated and saturated fatty acids were different. Photo-oxidation of stearic acid (saturated) did not induce any changes in the structure of the fatty acid. Only decrease in sp³ carbons and carbon in carboxylic groups (marked as O-C=O) was observed (Fig. 42 (a)). Thus, in case of this saturated fatty acid no other chemical changes than shortening of the alkyl chain resulting finally in total mineralization of the molecule was detected during photo-oxidation.

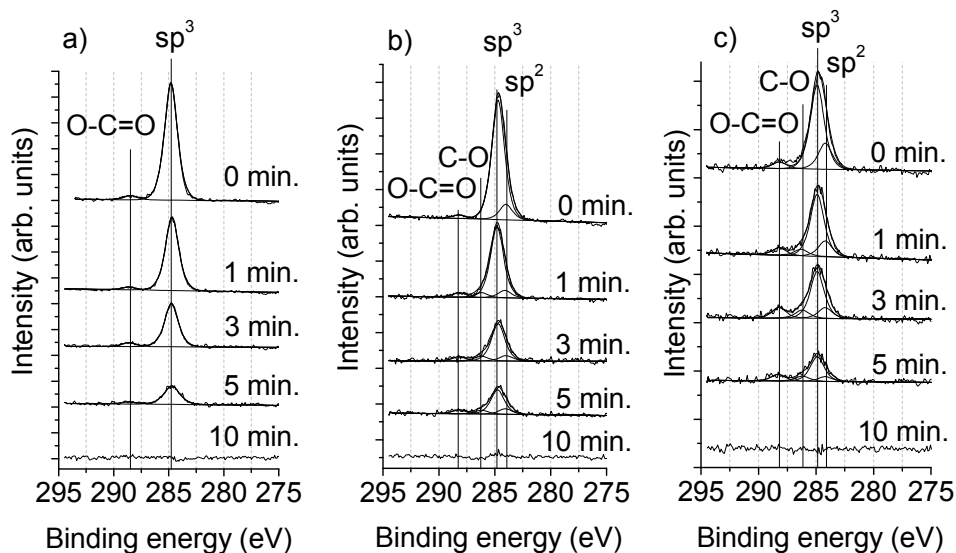


Figure 42. C 1s photo-lines of stearic (a), oleic (b) and linoleic (c) acid and change in their chemical composition and intensity after exposure to UV-A illumination on titania thin nanoparticle based films [V].

However, photo-oxidation of oleic (Fig. 42 (b)) and linoleic acid (Fig. 42 (c)) (both unsaturated) was different due to the radical reactions associated with carbon double bond. In the C 1s spectra of oleic and linoleic acid a shoulder related to C-O bond [114, 102] appeared at 286.2 ± 0.1 eV already after 1 min of UV-illumination. The appearance of C-O bonds during photo-oxidation of unsaturated fatty acids can be linked to the formation of peroxides, as is proposed by several authors [120, 121, 122]. Formation of peroxides in oleic and linoleic acids was most likely driven by $\bullet\text{OH}$ radicals (created by TiO_2 during UV-A irradiation) attacking a hydrogen atom in R-H and by that, creating a carbon radical $\text{R}\bullet$. In the next step, molecular oxygen is added to $\text{R}\bullet$ creating a peroxy radical $\text{ROO}\bullet$. Peroxy radical abstracts a hydrogen from the R-H bond creating a lipid hydroperoxide ROOH . Each lipid hydroperoxide contains one C-O bond between carbon and oxygen [121]. Formation of C-O bond was relatively fast: during the first three minutes of photo-oxidation the relative number of C-O bonds in oleic and linoleic acid layers increased (Fig. 43 (b) and Fig. 43 (c)), and then started to decrease as the total carbon composition decreased due to photo-oxidation. After 3 min of exposure the amount of C-O carbon became similar to the remaining amount of sp^2 carbon for both oleic and linoleic acid layers indicating that the change in the chemical composition of unsaturated fatty acids was quite extensive. One $\bullet\text{OH}$ radical can initiate a process resulting in peroxidation of several fatty acids (radical chain reaction); thus, even very low concentrations of $\bullet\text{OH}$ radicals can cause significant oxidative damage to the components of bacterial cellular membrane. The time

required for total photo-mineralization was similar for all three fatty acids. After 10 min of exposure to UV-illumination on nano-TiO₂ thin film the peaks for all carbon compounds had disappeared in the XPS spectra suggesting total mineralization of fatty acids.

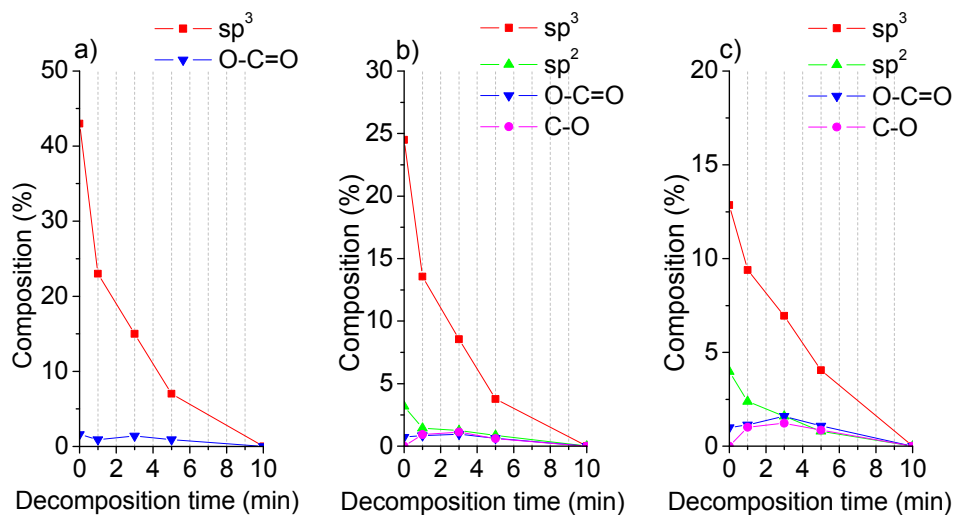


Figure 43. Decomposition of stearic (a), oleic (b) and linoleic (c) acid and change in their chemical composition after their exposure to UV-A illumination on titania thin nanoparticle based films [VI].

As stearic, oleic and linoleic acids are the main components of bacterial membranes [113, 123] it can be suggested that the chemical changes observed in XPS analysis of fatty acids could also take place in living cells when exposed to UV-activated TiO₂. The experiments with fatty acids suggest that in short time, saturated fatty acids will mineralize and unsaturated fatty acids will change in chemical composition and mineralize. Changes and rapid decomposition of fatty acids is probably the reason behind fast inactivation of *E. coli* on titania nanoparticle based thin films (Fig. 44), making the nanoparticle based thin films an effective self-cleaning and disinfecting system. In microbiology, colony-forming units per milliliter (CFU/ml) is a rough estimate of the number of bacteria able to form colonies in bacterial suspensions *i.e.* regarded as viable. Cell viability tests were used due to their simplicity and their ability to describe the surface from the standpoint of the application as a self-cleaning antibacterial surface.

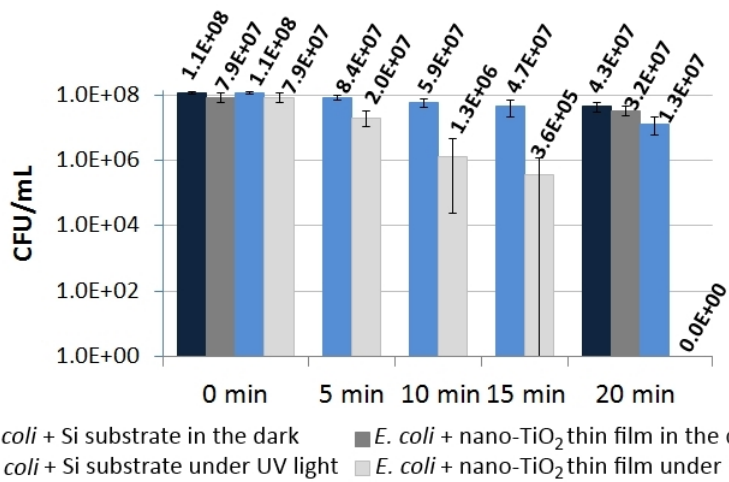


Figure 44. Colony forming potential of *E. coli* in different exposure conditions. The effect of UV-irradiation length on colony forming potential of *E. coli* applied onto silicon substrates (blue) or titania thin nanoparticle based films (grey) [VI].

Good photo-induced properties of the nanoparticle based films are most likely caused by the extremely high specific surface area of such films. Surface region of titania can trap photoholes, photoelectrons are effectively trapped by surface adsorbed oxygen [13] increasing the lifetime of photo-generated electron hole pairs.

5 CONCLUSIONS

Sol-gel method was used to prepare titania thin films directly or to synthesize anatase nanoparticles, which were used afterwards for nanoparticle based thin film preparation. The sol-gel films were doped with cobalt, nickel and copper and the effects of doping and different annealing temperatures were systematically investigated using different techniques. It is important to note that scientific community uses the word “doping” in narrower (semiconductor physics) and wider meaning. In the present work word “doping” is used in very general sense, *i.e.* as synonym for “introducing impurity element to the system”.

During annealing of sol-gel thin films several different processes occur simultaneously and all of them will contribute to the formation of the structure and chemical composition of the films. It was shown that at first the sol-gel films during annealing dry, organic material evaporates and oxidizes, the structure of the film becomes denser. Increasing temperature anatase crystalline structure starts to appear around 300-450 °C, and the phase transition from anatase to rutile crystal phase occurs above 700 °C.

Two different experimental techniques were used to study segregation of impurity: XPS to determine the changes in the chemical composition of the film surfaces and EDX to determine the elemental distribution of the films in horizontal dimensions. Both experiments demonstrated the segregation of the doping element, XPS results show that the concentration of the doping elements increases in the surface region during annealing and EDX measurements show horizontal segregation of the doping element into dopant rich regions. Probably both of the experiments describe two sides of the same process. It was demonstrated that exact crystal phase transition temperature and extent are highly dependent on the doping element and the substrate pre-treatment.

It was shown that also extent of segregation and the critical temperature, when the segregation starts depend on the type of the impurity element and pre-treatment of substrates. One of the driving forces behind the segregation might be oxidation state differences between the impurity atom and Ti^{4+} . The most common oxidation states in compounds are for nickel +2, +3, for cobalt +2, +3 and for copper +1, +2. For example when Ti^{4+} ion is replaced in the lattice by Ni^{2+} ion the charge difference has to be compensated. Segregation of nickel and cobalt out of titania matrix can be also drive by a second reason, namely formation of NiTiO_3 from TiO_2 and NiO (or CoTiO_3 from TiO_2 and CoO) is thermodynamically feasible in the temperature range used in this study. The appearance of NiTiO_3 and CoTiO_3 in the samples coincides well with the segregation of nickel and cobalt to the surface of the thin films. The system is complicated and it is likely that also other factors contribute to the segregation process of the impurity element out of titania matrix.

It was demonstrated that addition of doping element shifts the optical absorption edge of the material to lower energies or creates additional absorption bands in the visible region. The shifts of the absorption edge and additional absorbance in the visible region are probably due to the creation of

additional states by the impurity atom in the electronic structure of titania. The influence of secondary compounds and crystal phase shift from anatase to rutile (different band gaps) can influence the optical properties of the films and cannot be neglected. For example the band gaps of NiTiO_3 , CoTiO_3 and CuO are in the visible region and will also contribute to the absorbance in the doped titania thin films in the visible region. It was demonstrated that transition metal doping modifies the optical absorbance of titania thin films, though the positive effects to photoactivity of the material are not extensive. The most probable explanation for that is the formation of regions with increased metal concentrations during heating of samples. That means metal impurities do not appear in a regular TiO_2 crystal lattice but completely new system is formed. However, theoretical predictions about improvement of hydrophilic and photocatalytic properties are based on standpoint of single metal impurity atoms in regular TiO_2 crystal. The inhibition of light-induced hydrophilic properties on nickel and cobalt doped titania thin sol-gel films might also be due to the blocking of titania surface by inactive nickel and cobalt rich compounds.

Therefore it is still reasonable to continue investigations of doped TiO_2 , but most probably sol-gel process which includes heating at rather high temperatures is not the best method for preparation of metal doped TiO_2 samples with homogeneous impurity distribution.

It was demonstrated in the present work, that segregation of the doping element can be avoided by sodium impurities in the TiO_2 thin films. When segregation of the doping element is avoided, naturally hydrophilic surfaces can be achieved, though sodium impurities also destroy the crystalline structure of titania resulting in adverse effects to photoactivity of the material.

In the case of titania nanoparticle based thin films the crystalline structure (anatase) and surface morphology are determined by the synthesis of titania nanoparticles. With nanoparticle based systems extremely high specific surface areas of the films can be achieved. Also the temperature needed in post-treatment for achieving good photo-induced properties is considerably lower than for sol-gel titania thin films. Annealing of titania anatase nanoparticle films is necessary to adhere films to the substrate and to remove organic material from the films. In contrast to sol-gel titania thin films which achieve greatest activity after being annealed at $550\text{ }^\circ\text{C}$, titania nanoparticle based thin films can be used already after annealing at $400\text{ }^\circ\text{C}$. Both, good photoactivity and low treatment temperature are very important for improvement of industrial application and cost-effectiveness of TiO_2 based materials. Titania nanoparticle thin films show good photo-induced properties even with low UV-A irradiation intensities and could be used in normal sunlight conditions as self-cleaning and bactericidal surfaces.

It was shown that the titania anatase nanoparticles based thin films exhibit high photocatalytic activity and rapidly decompose different fatty acids on the surface of the films. Investigated fatty acids are important components of bacterial cell membrane, but also extremely good model contaminants. It was demonstrated that during decomposition also the chemical nature of unsaturated

fatty acids changes. Chemical changes and rapid decomposition of fatty acids is the reason behind fast inactivation of *E. coli* bacteria on titania nanoparticle based thin films, showing that these are effective self-cleaning and disinfecting systems. This system could be easily scaled up and used to coat large surfaces, due to the simplicity of the nanoparticle based film preparation and easy handling of the nanoparticle dispersions. The high effectiveness of the nanoparticle based films in lighting conditions comparable to the sunlight, is especially interesting for potential future applications.

6 KOKKUVÕTE

Lisandist ja valmistamistingimustest sõltuvad õhukeste TiO₂ kilede omadused

Antud töös kasutati sool-geel meetodit õhukeste TiO₂-kilede valmistamiseks. Kilesid dopeeriti koobalti, nikli ja vasega ning kasutades erinevaid meetodeid uuriti süstemaatiliselt lisandite ning kuumutamisrežiimi mõju kilede struktuurile, morfoloogiale ja omadustele. Alternatiivselt kasutati sool-geel meetodit esmalt nanoosakeste valmistamiseks ja seejärel valmistati nendest nanoosakestest õhukesi TiO₂-kilesid. Antud töö kontekstis on veel oluline märkida, et terminit “dopeerima“ kasutatakse teaduskirjanduses nii kitsamas tähenduses (pooljuhtide füüsika) kui ka laiemas tähenduses. Käesolevas töös kasutatakse väljendit “dopeerimine” justnimelt laiemas mõttes, s.t. tähenduses “lisandi süsteemi viimine”.

Sool-geel kilede kuumutamisel muutub nii kilede keemiline koostis kui ka struktuur. Antud töös näidati, et temperatuuri järkjärgulisel tõstmisel aurustuvad kõigepealt lenduvad orgaanilised ühendid, seejärel hakkavad toimuma oksüdatsiooniprotsessid, kiled muutuvad tihedamaks. Edasisel kuumutamisel ilmub kristallstruktuur (alates 300–450 °C, anataas) ning veelgi kõrgematel kuumutustemperatuuridel (700 °C ja kõrgematel) toimub faasisiire anataasist rutiiliks. Näidati, et faasisiirde temperatuurid sõltuvad nii lisandist kui ka kilede aluste eeltötlusest.

Näidati, et kuumutamise käigus segregeerub algselt homogeenelt jaotunud dopant TiO₂ maatriksist välja. Dopandi liikumist kilede sügavamatest piirkondadest objekti pinna suunas jälgiti XPS-i abil. Dopandi segregatsiooni kilede pinnal – s.t. kõrgendatud dopandi sisaldusega piirkondade formeerumist horisontaalsel tasandil aga EDX-i abil. Ilmselt on tegu sama protsessi erinevate ilmingutega.

Segregatsiooni ulatus ja temperatuur, millest alates segregatsioon toimuma hakkab, sõltuvad nii lisandist kui ka aluse eeltötlusest. Segregatsiooni üheks põhjuseks on dopandi oksüdatsiooniastme erinevus Ti⁴⁺ ionide oksüdatsiooniastmest. Nimelt on Ti⁴⁺ asendamisel nikli, vase või koobaltiga vaja kompenseerida tekkiv laengute erinevus. Samuti on termodünaamiliselt soodne nikkel ja koobalt titanaatide moodustumine ja ka see võib lisandite segregatsioonile kaasa aidata. NiTiO₃ ja CoTiO₃ tekkimise temperatuur kuumutamise käigus langeb hästi kokku segregatsiooni protsessi alguse temperatuuriga. Tuleb silmas pidada, et tegu on keeruliste süsteemidega ning lisandite segregatsiooni TiO₂ maatriksis mõjutavad arvatavasti mitmed tegurid.

Näidati, et dopeeriva elemendi lisamisega on võimalik kilede optilist neeldumisäärt nihutada väiksemate footoni energiatega poole või tekitada täiendavat neeldumist nähtavas piirkonnas. Neeldumisääre nihe on ilmselt põhjustatud TiO₂ elektronstruktuuris tekkivatest lisandi nivoodest. Samuti võivad mõju avaldada nii faasiüleminekud anataasist rutiili kui ka NiTiO₃ ja CoTiO₃ ning vask oksiidi tekkimine. Kõigi eelmainitud ühendite keelutsoonid

on piisavalt kitsad, et mõjutada nähtava valguse neeldumist. Suurenenud neeldumisele vaatamata ei parandanud dopeerimine märkimisväärselt kilede fotoaktiivseid omadusi. Põhjuseks võis olla lisandi segregatsioon: dopant ei asendanud TiO₂ võres Ti⁴⁺ ioone vaid kogunes kõrgendatud lisandi sisaldusega regioonidesse ning moodustus täiesti uus süsteem. Enamus kirjanduses kättesaadavaid tsooniarvutusi on aga tehtud süsteemide kohta, kus dopandi ioonid asendavad Ti⁴⁺ ioone võres. Samuti on võimalik, et lisandi segregatsiooni käigus blokeeritakse pind mitte-fotoaktiivsete ühendite poolt.

Eelnevast võib järeldada, et fotokatalüütiliste pindade valmistamise uurimine on jätkuvalt aktuaalne, kuid arvatavasti ei ole sool-geel meetod metalliga ühtlaselt dopeeritud TiO₂ kilede valmistamiseks sobivaim. Kõrgetel temperatuuridel kuumutamine on selle meetodi puhul vajalik fotoaktiivse anataasi kristallstruktuuri formeerimiseks, kuid samas põhjustab kuumutamine lisandi segregatsiooni TiO₂ maatriksist kõrge metallisisaldusega regioonidesse.

Käesolevas töös näidati, et dopandi ühtlast jaotust maatriksis on võimalik saavutada naatriumi lisandi abil, mis aitab kaasa ka iseeneslikult hüdrofiilsete pindade tekkele. Samas hävitab naatrium fotoaktiivse anataasi faasi ja mõjutab pindade fotokatalüütilist aktiivsust negatiivselt.

Käesolevas töös uuriti alternatiivselt ka TiO₂ nanoosakestest valmistatud kilesid, mis on kristallilised (anataasi faasis) juba enne kuumutamist. Selliste kilede omadused on määratud suures osas sünteesitud nanoosakeste omadustega ja nende kilede puhul on võimalik saavutada suurt eripinda. Selliste kilede valmistamisjärgsed kuumutustemperatuurid fotoaktiivsete omaduste saavutamiseks on võrreldes sool-geel kiledega madalamad. Kui sool-geel meetodil valmistatud õhukeste TiO₂ kilede puhul saabub kõige tugevam fotoaktiivsus kuumutustemperatuuri 550 °C juures, siis nanoosakestel baseeruvate kilede korral on vajalik kuumutustemperatuur 400 °C. Oluline on seejuures märkida, et kuna nanoosakesed on juba algusest peale anataasi faasis, siis nanoosakestel baseeruvate kilede korral on kuumutamine vajalik sidumaks nanoosakesi substraadi külge ja orgaanilise materjali eemaldamiseks.

Antud töös näidati, et TiO₂ nanoosakestest valmistatud kiled suudavad väga efektiivselt lagundada nii rasvhappeid kui ka hävitada *Escherichia coli* baktereid. Rasvhapped on väga heaks mudeliks määratud pindade imiteerimisel, samuti on need bakterite membraanide olulised koostisosad ja nende lagundamise mehhanismide uurimine võimaldab seega saada infot TiO₂ pinna antibakteriaalsete mehhanismide kohta. Nanoosakestest valmistatud TiO₂ kiled osutusid efektiivseks isegi väikese footoni energiaga UV-A valgusega aktiveerimisel. Juba lühikese valgustamise jooksul võis jälgida keemilisi muutusi TiO₂ kiledele kantud rasvhapetes ning 10 minuti jooksul oksüdeeriti kogu pinnale kantud rasvhape.

Seega võib antud töö tulemuste põhjal väita, et TiO₂ nanoosakestest valmistatud kilede madalad töötlemistemperatuurid, head fotokatalüütilised omadused ning lihtne valmistamismetoodika teevad neist perspektiivika materjali tööstuslikeks rakendusteks.

ACKNOWLEDGEMENTS

I would like to thank the following persons for their support and help during the preparation of this work: Vambola Kisand, Meeri Visnapuu, Angela Ivask, Anne Kahru, Katre Juganson, Leonard Matisen, Rainer Pärna, Ergo Nõmmiste, and everybody else who contributed to this work.

I acknowledge the following agencies and foundations for the financial support: Graduate School “Functional Materials and Technologies” (European Social Fund project 1.2.0401.09-0079), Estonian Research Council (target-financed theme IUT2-25, grants 8216, 8737 and 7615); Estonian Nanotechnology Competence Center (EU29996); ERDF projects (“IRGLASS” 3.2.1101.12-0027, “TRIBOFILM” 3.2.1101.12-0028, “Nano-Com” 3.2.1101.12-0010, “Mesosystems: Theory and Applications” TK114, “High-technology Materials for Sustainable Development“ TK117); Development Fund of University of Tartu.

REFERENCES

- [1] M. Keshmiri, M. Mohseni, T. Troczynski, "Development of novel TiO₂ sol-gel-derived composite and its photocatalytic activities for trichloroethylene oxidation," *Appl. Catal. B: Environ.*, vol. 53, pp. 209–219, 2004.
- [2] G. M. Kiema, M. J. Colgan, and M. J. Brett, "Dye sensitized solar cells incorporating obliquely deposited titanium oxide layers," *Solar Energy Mater. Solar Cells*, vol. 85, pp. 321–331, 2005.
- [3] T. J. Webster, R. W. Siegel, and R. Bizios, "Osteoblast adhesion on nanophase ceramics," *Biomater.*, vol. 20, pp. 1221–1227, 1999.
- [4] R. Wang, K. Hashimoto, A. Fujishima, M. Chikuni, E. Kojima, A. Kitamura, M. Shimohigoshi, T. Watanabe, "Light-induced amphiphilic surfaces," *Nature*, vol. 388, pp. 431–432, 1997.
- [5] R. Wang, K. Hashimoto, A. Fujishima, M. Chikuni, E. Kojima, A. Kitamura, M. Shimohigoshi, and T. Watanabe, "Photogeneration of highly amphiphilic TiO₂ surfaces," *Adv. Mater.*, vol. 10, pp. 135–138, 1998.
- [6] Z. Zhang, C. Wang, R. Zakaria, J. Y. Ying, "Role of particle size in nanocrystalline TiO₂-based photocatalysts," *J. Phys. Chem. B*, vol. 102, pp. 10871–10878, 1998.
- [7] E. Stathatos, P. Lianos, C. Tsakiroglou, "Highly efficient nanocrystalline titania films made from organic/inorganic nanocomposite gels," *Microporous Mesoporous Mater.*, vol. 75, pp. 255–260, 2004.
- [8] A. Fujishima, K. Honda, "Electrochemical photolysis of water at a semiconductor electrode," *Nature*, vol. 238, pp. 37–38, 1972.
- [9] C. M. Visinescu, R. Sanjines, F. Levy, and V. I. Parvulescu, "Photocatalytic degradation of acetone by Ni-doped titania thin films prepared by dc reactive sputtering," *Appl. Catal. B: Environ.*, vol. 60, pp. 155–162, 2005.
- [10] Y. Lim, J. Jeong, J. An, Y. Jeon, K. Jeon, K. Hwang, B. Kim, "Nickel-doped titanium oxide films prepared by chemical solution deposition," *J. Ceram. Proc. Res.*, vol. 6, pp. 302–304, 2005.
- [11] C. E. Rodriguez Torres, A. F. Cabrera, L. A. Errico, S. Duhalde, M. Renteria, F. Golmar, F. H. Sanchez, "XAS study of the local environment of impurities in doped TiO₂ thin films," *Physica B*, vol. 398, pp. 219–222, 2007.
- [12] S. D. Sharma, D. Singh, K. K. Saini, C. Kant, V. Sharma, S. C. Jain, C. P. Sharma, "Sol-gel-derived super-hydrophilic nickel doped TiO₂ film as active photo-catalyst," *Appl. Catal. A: Gen.*, vol. 314, pp. 40–46, 2006.
- [13] O. Carp, C. L. Huisman, A. Reller, "Photoinduced reactivity of titanium dioxide," *Prog. Solid State Chem.*, vol. 32, pp. 33–177, 2004.
- [14] S. Rehman, R. Ullah, A. M. Butt, N. D. Gohar, "Strategies of making TiO₂ and ZnO visible light active," *J. Hazard. Mater.*, vol. 170, pp. 560–569, 2009.
- [15] C. D. Valentin, E. Finazzi, G. Pacchioni, A. Selloni, S. Livraghi, M. C. Paganini, E. Giamello, "N-doped TiO₂: theory and experiment," *Chem. Phys.*, vol. 339, pp. 44–56, 2007.
- [16] A. Iwaszuk, M. Nolan, Q. Jin, M. Fujishima, H. Tada, "Origin of the Visible-Light Response of Nickel(II) oxide cluster surface modified titanium(IV) dioxide," *J. Phys. Chem. C*, vol. 117, pp. 2709–2718, 2013.
- [17] J. Liveage, M. Henry, C. Sanchez, "Sol-Gel chemistry of transition metal oxides," *Prog. Solid State Ch.*, vol. 18, pp. 259–342, 1988.

- [18] M. J. Velasco, F. Rubio, J. Rubio, J.L. Oteo, "DSC and FT-IR analysis of the drying process of titanium alkoxide derived precipitates," *Thermochim Acta*, vol. 326, pp. 91–97, 1999.
- [19] M. T. Harris, A. Singhal, J. L. Look, J. R. Smith-Kristensen, J. S. Lin, L. M. Toth, "FTIR spectroscopy, SAXS and electrical conductivity studies," *J. Sol-Gel Sci. Techn.*, vol. 8, pp. 41–47, 1997.
- [20] J. Blanchard, M. In, B. Schaudel, C. Sanchez, "Hydrolysis and Condensation Reactions of Transition Metal Alkoxides: Calorimetry study and evaluation of the extent of reaction.," *Eur. J. Inorg. Chem*, vol. 1998, pp. 1115–1127, 1998.
- [21] J. Jögi, M. Järvekülg, J. Kalda, A. Salundi, V. Reedo, A. Lõhmus, "Simulation of cracking of metal alkoxide gel film formed on viscous precursor layer using a spring-block model," *EPL*, vol. 95, pp. 64005, 2011.
- [22] R.A Zoppi, B.C Trasferetti, C.U Davanzo, "Sol-gel titanium dioxide thin films on platinum substrates: preparation and characterization," *J. Electroanal. Chem.*, vol. 544, pp. 47–57, 2003.
- [23] N. Negishi, K. Takeuchi, "Structural changes of transparent TiO₂ thin films with heat treatment," *Mater. Lett.*, vol. 38, pp. 150–153, 1999.
- [24] J. Yu, J. C. Yu, W. Ho, Z. Jiang, "Effects of calcination temperature on the photocatalytic activity and photo-induced super-hydrophilicity of mesoporous TiO₂ thin films," *New J. Chem.*, vol. 26, pp. 607–613, 2002.
- [25] N. Wetchakun, S. Phanichphant, "Effect of temperature on the degree of anatase-rutile transformation in titanium dioxide nanoparticles synthesized by the modified sol-gel method," *Curr. Appl. Phys.*, vol. 8, pp. 343–346, 2008.
- [26] R. Arroyo, G.Cordoba, J. Padilla, V.H. Lara, "Influence of manganese ions on the anatase-rutile phase transition of TiO₂ prepared by the sol-gel process," *Mater. Lett.*, vol. 54, pp. 397–402, 2002.
- [27] P. Cheng, M. Zheng, Y. Jin, Q. Huang, M. Gu, "Preparation and characterization of silica-doped titania photocatalyst through sol-gel method," *Mater. Lett.*, vol. 57, pp. 2989–2994, 2003.
- [28] Y.-H. Zhang, A. Reller, "Phase transformation and grain growth of doped nanosized titania," *Mater. Sci. Eng. C*, vol. 19, pp. 323–326, 2002.
- [29] M. Yoshinaka, K. Hirota, O. Yamaguchi, "Formation and sintering of TiO₂ (Anatase) solid solution in the system TiO₂-SiO₂," *J. Am. Ceram. Soc.*, vol. 80, pp. 2749–2753, 1997.
- [30] L. M. Nikolić, L. Radonjić, V. V. Srdić, "Effect of substrate type on nanostructured titania sol-gel coatings for sensors applications," *Ceram. Int.*, vol. 31, pp. 261–266, 2005.
- [31] A. Verma, S.A. Agnihotry, "Thermal treatment effect on nanostructured TiO₂ films deposited using diethanolamine stabilized precursor sol," *Electrochim. Acta*, vol. 52, pp. 2701–2709, 2007.
- [32] E. Scholan, C. Sanchez, "Synthesis and Characterization of surface-protected nanocrystalline titania particles," *Chem. Mater.*, vol. 10, pp. 3217–3223, 1998.
- [33] M. Niederberger, M.H. Bartl, G.D. Stucky, "Benzyl alcohol and transition metal chlorides as a versatile reaction system for the nonaqueous and low-temperature synthesis of crystalline nano-objects with controlled dimensionality," *J. Am. Chem. Soc.*, vol. 124, pp. 13642–13643, 2002.
- [34] M. Niederberger, M.H. Blart, G.D. Stucky, "Benzyl alcohol and titanium tetrachloride a versatile reaction system for the nonaqueous and low-temperature preparation of crystalline and luminescent titania nanoparticles," *Chem. Mater.*, vol. 14, pp. 4364–4370, 2002.

- [35] A. Vioux, "Nonhydrolytic sol-gel routes to oxides," *Chem. Mater.*, vol. 9, pp. 2292-2299, 1997.
- [36] D. Meyerhofer, "Characteristics of resist films produced by spinning," *J. Appl. Phys.*, vol. 49, pp. 3993-3997, 1978.
- [37] C. J. Lawrence, "The mechanics of spin coating of polymer films," *Phys. Fluids*, vol. 31, pp. 2786-2795, 1988.
- [38] B. J. Norris, J. Anderson, J. F. Wager, D. A. Keszler, "Spin-coated zinc oxide transparent transistors," *J. Phys. D: Appl. Phys.*, vol. 36, pp. L105-L107, 2003.
- [39] P. Jiang, M. J. McFarland, "Large-scale fabrication of wafer-size colloidal crystals, macroporous polymers and nanocomposites by spin-coating," *J. Am. Chem. Soc.*, vol. 126, pp. 13778-13786, 2004.
- [40] D. B. Hall, P. Underhill, J. M. Torkelson, "Spin coating of thin and ultrathin polymerfilms," *Polym. Eng. Sci.*, vol. 38, pp. 2039-2045, 1998.
- [41] W. Choi, A. Termin, M. R. Hoffmann, "The role of metal ion dopants in quantum-sized TiO₂: correlation between photoreactivity and charge carrier recombination dynamics," *J. Phys. Chem.*, vol. 98, pp. 13669-13679, 1994.
- [42] J. Zhou, Y. Zhang, X. S. Zhao, A. K. Ray, "Photodegradation of benzoic acid over metal-doped TiO₂," *Ind. Eng. Chem. Res.*, vol. 45, pp. 3503-3511, 2006.
- [43] M. Ni, M. K.H. Leung, D. Y.C. Leung, K. Sumathy, "A review and recent developments in photocatalytic water-splitting using TiO₂ for hydrogen production," *Renew. Sust. Energ. Rev.*, vol. 11, pp. 401-425, 2007.
- [44] J. Chen, L. Eberlein, C. H. Langford, "Pathways of phenol and benzene photo-oxidation using TiO₂ supported on a zeolite," *J. Photoch. Photobio. A*, vol. 148, pp. 183-189, 2002.
- [45] M. Anpo, T. Shima, S. Kodama, Y. Kubokawa, "Photocatalytic Hydrogenation of CH₃CCH with H₂O on Small-Particle TiO₂: Size quantization effects and reaction intermediates," *J. Phys. Chem.*, vol. 91, pp. 4305-4310, 1987.
- [46] M. Styliidi, D. I. Kondarides, X. E. Verykios, "Pathways of solar light-induced photocatalytic degradation of azo dyes in aqueous TiO₂ suspensions," *Appl. Catal. B-enviro.*, vol. 40, pp. 271-286, 2003.
- [47] A. Fujishima, X. Zhang, D. A. Tryk, "TiO₂ photocatalysis and related surface phenomena," *Surf. Sci. Rep.*, vol. 63, pp. 515-582, 2008.
- [48] Y. Mao, C. Schoneich, K.-D. Asmus, "Identification of organic acids and other intermediates in oxidative degradation of dchlorinated ethanes on TiO₂ surfaces en route to mineralization. A combined photocatalytic and radiation chemical study," *J. Phys. Chem.*, vol. 95, pp. 10080-10089, 1991.
- [49] S. Kim, W. Choi, "Kinetics and mechanisms of photocatalytic degradation of (CH₃)_nNH_{4-n} (0<n<4) in TiO₂ suspension: the role of OH radicals," *Environ. Sci. Technol.*, vol. 36, pp. 2019-2025, 2002.
- [50] M. Cho, H. Chung, W. Choi, J. Yoon, "Linear correlation between inactivation of E. coli and OH radical concentration in TiO₂ photocatalytic disinfection," *Water Res.*, vol. 38, pp. 1069-1077, 2004.
- [51] M. C. Lee, W. Choi, "Solid phase photocatalytic reaction on the soot/TiO₂ interface: the role of migrating OH radicals," *J. Phys. Chem. B*, vol. 106, pp. 11818-11822, 2002.
- [52] T. Tachikawa, S. Tojo, M. Fujitsuka, T. Majima, "Influences of adsorption on TiO₂ photocatalytic one-electron oxidation of aromatic sulfides studied by time-resolved diffuse reflectance spectroscopy," *J. Phys. Chem. B*, vol. 108, pp. 5859-5866, 2004.

- [53] R. B. Draper, M. A. Fox, "Titanium dioxide photosensitized reactions studied by diffuse reflectance flash photolysis in aqueous suspensions of TiO₂ powder," *Langmuir*, vol. 6, pp. 1396–1402, 1990.
- [54] A. Fujishima, T. N. Rao, D. A. Tryk, "Titanium dioxide photocatalysis," *J. Photochem. Photobiol. C*, vol. 1, pp. 1–21, 2000.
- [55] R. Wang, K. Hashimoto, A. Fujishima, M. Chicuni, E. Kojima, A. Kitamura, M. Shimohigoshi, T. Watanabe, "Light-induced amphiphilic surfaces," *Nature*, vol. 388, pp. 431–432, 1997.
- [56] R-D. Sun, A. Nakajima, A. Fujishima, T. Watanabe, K. Hashimoto, "Photo-induced surface wettability conversion of ZnO and TiO₂ thin films," *J. Phys. Chem. B*, vol. 105, pp. 1984–1990, 2001.
- [57] M. Miyauchi, A. Nakajima, A. Fujishima, K. Hashimoto, T. Watanabe, "Photo-induced surface reactions on TiO₂ and SrTiO₃ films: photocatalytic oxidation and photoinduced hydrophilicity," *Chem. Mater.*, vol. 12, pp. 3–5, 2000.
- [58] X. Yan, R. Abe, T. Ohno, M. Toyofuku, B. Ohtani, "Action spectrum analyses of photoinduced superhydrophilicity of titania thin films on glass plates," *Thin Solid Films*, vol. 516, pp. 5872–5876, 2008.
- [59] T. Zubkov, D. Stahl, T. L. Thompson, D. Panayotov, O. Diwald, J. T. Yates, "Ultraviolet light-induced hydrophilicity effect on TiO₂ (110)(1x1). Dominant role of the photooxidation of adsorbed hydrocarbons causing wetting by water droplets," *J. Phys. Chem. B*, vol. 109, pp. 15454 -15462, 2005.
- [60] J. M. White, J. Szanyi, M. A. Henderson, "The photon-driven hydrophilicity of titania: a model study using TiO₂(110) and adsorbed trimethyl acetate," *J. Phys. Chem. B*, vol. 107, pp. 9029–9033, 2003.
- [61] M. Miyauchi, A. Nakajima, T. Watanabe, K. Hashimoto, "Photocatalysis and photoinduced hydrophilicity of various metal oxide thin films," *Chem. Mater.*, vol. 14, pp. 2812–2816, 2002.
- [62] H. Tang, K. Prasad, R. Sanjines, P. E. Schmid, F. Levy, "Electrical and optical properties of TiO₂ anatase thin films.," *J. Appl. Phys.*, vol. 75, pp. 2042–2047, 1994.
- [63] J. Mozer, M. Grätzel, "Photosensitized electron injection in colloidal semiconductors," *J. Am. Chem. Soc.*, vol. 106, pp. 6557–6464, 1984.
- [64] D. Chatterjee, S. Dasgupta, "Visible light induced photocatalytic degradation of organic pollutants," *J. Photoch. Photobio. C*, vol. 6, pp. 186–205, 2005.
- [65] P. V. Kamat, J-P. Chauvet, R. W. Fessenden, "Photoelectrochemistry in particulate systems 4. photosensitization of a TiO₂ semiconductor with a chlorophyll analogue," *J. Phys. Chem.*, vol. 90, pp. 1389–1394, 1986.
- [66] J. Hodak, C. Quinteros, M. I. Litter, E. S. Roman, "Sensitization of TiO₂ with phthalocyanines part 1.- Photooxidations using hydroxoaluminium tricarboxy-monoamidephthalocyanine adsorbed on TiO₂," *J. Chem. Soc., Faraday Trans.*, vol. 92, pp. 5081–5088, 1996.
- [67] D. Jianga, Y. Xu, B. Hou, D. Wu, Y. Sun, "Synthesis of visible light-activated TiO₂ photocatalyst via surface organic modification," *J. Solid State Chem.*, vol. 180, pp. 1787–1791, 2007.
- [68] M. Li, P. Tang, Z. Hong, M. Wang, "High efficient surface-complex-assisted photodegradation of phenolic compounds in single anatase titania under visible-light," *Colloid. Surface A*, vol. 318, pp. 285–290, 2008.
- [69] C. D. Valentin, G. Pacchioni, A. Selloni, S. Livraghi, E. Giamello, "Characterization of paramagnetic species in N-Doped TiO₂ powders by EPR spectroscopy and DFT calculations," *J. Phys. Chem. B*, vol. 109, pp. 11414–11419, 2005.

- [70] M. Subramaniana, S. Vijayalakshmi, S. Venkataraja, R. Jayavel, "Effect of cobalt doping on the structural and optical properties of TiO₂ films prepared by sol-gel process," *Thin Solid Films*, vol. 516, pp. 3776–3782, 2008.
- [71] S. George, S. Pokhrel, Z. Ji, B. L. Henderson, T. Xia, L. J. Li, "Role of Fe doping in tuning the band gap of TiO₂ for the photo-oxidation-induced cytotoxicity paradigm," *J. Am. Chem. Soc.*, vol. 133, pp. 11270–11278, 2011.
- [72] K. Nagaveni, M. S. Hegde, G. Madras, "Structure and photocatalytic activity of Ti_{1-x}M_xO_{2+d} (M=W, V, Ce, Zr, Fe, and Cu) synthesized by solution combustion method," *J. Phys. Chem. B*, vol. 108, pp. 20204–20212, 2004.
- [73] R. López, R. Gómez, M. E. Llanos, "Photophysical and photocatalytic properties of nanosized copper-doped titania sol-gel catalysts," *Catal. Today*, vol. 148, pp. 103–108, 2009.
- [74] T. Umebayashi, T. Yamaki, H. Itoh, K. Asai, "Analysis of structures of 3d transition metal-doped TiO₂ based on band calculations," *J. Phys. Chem. Solids*, vol. 63, pp. 1909–1920, 2002.
- [75] R.-A. Doong, C.-H. Chen, R.A. Maithreepala, S.-M. Chang, "The influence of pH and cadmium sulfide on the photocatalytic degradation of 2-chlorophenol in titanium dioxide suspensions," *Water Res.*, vol. 35, pp. 2873–2880, 2001.
- [76] M. G. Kang, H.-E. Han, K.-J. Kim, "Enhanced photodecomposition of 4-chlorophenol in aqueous solution by deposition of CdS on TiO₂," *J. Photoch. Photobio. A*, vol. 125, pp. 119–125, 1999.
- [77] W.-W. So, K.-J. Kim, S.-J. Moon, "Photo-production of hydrogen over the CdS–TiO₂ nano-composite particulate films treated with TiCl₄," *Int. J. Hydrogen Energ.*, vol. 29, pp. 229–234, 2004.
- [78] S. Hüfner, *Photoelectron Spectroscopy Principles and Applications*, Berlin, Heidelberg, New York, Hong Kong, London, Milan, Paris, Tokyo: Springer, 2003.
- [79] M.P. Seah, I.S. Gilmore, S.J. Spencer, "Background subtraction II. General behaviour of REELS and the Tougaard universal cross section in the removal of backgrounds in AES and XPS," *Surf. Sci.*, vol. 461, pp. 1–15, 2000.
- [80] Y. F. Chen, Y. T. Chen, "Background removal in surface electron spectroscopy: Influence of surface excitations," *Phys. Rev. B*, vol. 53, pp. 4980–4988, 1996.
- [81] C. J. Powell, J. M. Conny, "Evaluation of uncertainties in X-ray photoelectron spectroscopy intensities associated with different methods and procedures for background subtraction. I. Spectra for monochromatic Al X-ray," *Surf. Interface Anal.*, vol. 41, pp. 269–294, 2009.
- [82] C. J. Powell, J. M. Conny, "Evaluation of uncertainties in X-ray photoelectron spectroscopy intensities associated with different methods and procedures for background subtraction. II. Spectra for unmonochromated Al and Mg X-rays," *Surf. Interface Anal.*, vol. 41, pp. 804–813, 2009.
- [83] S. Tougaard, "Accuracy of the non-destructive surface nanostructure quantification technique based on analysis of the XPS or AES peak shape," *Surf. Interface Anal.*, vol. 26, pp. 249–269, 1998.
- [84] M. P. Seah, I. S. Gilmore, S. J. Spencer, "Quantitative XPS: I. analysis of X-ray photoelectron intensities from elemental data in a digital photoelectron database," *J. Electron Spectrosc.*, vol. 120, pp. 93–111, 2001.
- [85] N. Fairley, "CasaXPS version 2.3.12," 2000. Available: www.casaxps.com.
- [86] I.R. Beattie, T.R. Gilson, "Single crystal laser Raman spectroscopy," *Proc.R. Soc. London Ser. A*, vol. 307, pp. 407–429, 1968.

- [87] A. Li Bassi, D. Cattaneo, V. Russo, C. E. Bottani, E. Barborini, T. Mazza, P. Piseri, P. Milani, F. O. Ernst, K. Wegner, S. E. Pratsinis, "Raman spectroscopy characterization of titania nanoparticles produced by flame pyrolysis: the influence of size and stoichiometry," *J. Appl. Phys.*, vol. 98, pp. 074305, 2005.
- [88] M. I. Baraton, G. Busca, M. C. Prieto, G. Ricchiardi, V. S. Escribano, "On the vibrational spectra and structure of FeCrO₃ and of the ilmenite-type compounds CoTiO₃ and NiTiO₃," *J. Solid State Chem.*, vol. 112, pp. 9–14, 1994.
- [89] G. Busca, G. Ramis, J. M. G. Amores, V. S. Escribano, P. Piaggio, "FT Raman and FTIR studies of titanias and metatitanate powders," *J. Chem. Soc. Faraday Trans.*, vol. 90, pp. 3181–3190, 1994.
- [90] G. W. Zhou, D. K. Lee, Y. H. Kim, C. W. Kim, Y. S. Kang, "Preparation and spectroscopic characterization of ilmenite-type CoTiO₃ nanoparticles," *Bull. Korean Chem. Soc.*, vol. 27, pp. 368–372, 2006.
- [91] Z. H. Gan, G. Q. Yu, B. K. Tay, C. M. Tan, Z. W. Zhao, Y. Q. Fu, "Preparation and characterization of copper oxide thin films deposited by filtered cathodic vacuum arc," *J. Phys. D: Appl. Phys.*, vol. 37, pp. 81–85, 2004.
- [92] N. Dharmaraja, H. C. Park, C. K. Kim, H. Y. Kim, D. R. Lee, "Nickel titanate nanofibers by electrospinning," *Mater. Chem. Phys.*, vol. 87, pp. 5–9, 2004.
- [93] V. Gupta, K. K. Bamza, P. N. Kotru, B. M. Wanklyn, "Mechanical characteristics of flux-grown calcium titanate and nickel titanate crystals," *Mater. Chem. Phys.*, vol. 89, pp. 64–71, 2005.
- [94] F. Pacheco, M. Gonzalez, A. Medina, S. Velumani, J. A. Ascencio, "Structural analysis of cobalt titanate nanoparticles obtained by sol-gel process," *Appl. Phys. A*, vol. 78, pp. 531–536, 2004.
- [95] K. T. Jacob, V. S. Saji, S. N. S. Reddy, "Thermodynamic evidence for order-disorder transition in NiTiO₃," *J. Chem. Thermodynamics*, vol. 39, pp. 230–235, 2007.
- [96] K. T. Jacob, G. Rajitha, "Role of entropy in the stability of cobalt titanates," *J. Chem. Thermodynamics*, vol. 42, pp. 879–885, 2010.
- [97] E. Mack, G. G. Osterhof, H. M. Kraner, "Vapor pressure of copper oxide and of copper," *J. Am. Chem. Soc.*, vol. 45, pp. 617–623, 1923.
- [98] R. Lopez, R. Gomez, M. E. Llanos, "Photophysical and photocatalytic properties of nanosized copper-doped titania sol-gel catalysts," *Catal. Today*, vol. 2009, pp. 103–108, 148.
- [99] N. S. McIntyre, M. G. Cook, "X-ray photoelectron studies on some oxides and hydroxides of cobalt, nickel, and copper," *Anal. Chem.*, vol. 47, pp. 2208–2213, 1975.
- [100] G. van der Laan, C. Westra, C. Haas, G. A. Sawatzky, "Satellite structure in photoelectron and Auger spectra of copper dihalides," *Phys. Rev. B*, vol. 23, pp. 4369–4380, 1981.
- [101] M. C. Biesinger, L. W. M. Lau, A. R. Gerson, R. St. C. Smart, "Resolving surface chemical states in XPS analysis of first row transition metals, oxides and hydroxides: Sc, Ti, V, Cu and Zn," *Appl. Surf. Sci.*, vol. 257, pp. 887–898, 2010.
- [102] B. P. Payne, M. C. Biesinger, N. S. McIntyre, "X-ray photoelectron spectroscopy studies of reactions on chromium metal and chromium oxide surfaces," *J. Electron Spectrosc. Relat. Phenom.*, vol. 184, pp. 29–37, 2011.
- [103] G. Moretti, G. Fierro, M. Lo Jacono, P. Porta, "Characterization of CuO–ZnO catalysts by X-ray photoelectron spectroscopy: Precursors, calcined and reduced samples," *Surf. Interface Anal.*, vol. 14, pp. 325–336, 1989.

- [104] „Digitalfire Ceramic Materials Database,” Available: http://digitalfire.com/4sight/material/copper_hydroxide_2252.html.
- [105] National Renewable Energy Laboratory (U.S.), Available: <http://rredc.nrel.gov/solar/spectra/am1.5/>.
- [106] P. Vitanova, T. Babenova, Z. Alexieva, A. Harizanova, Z. Nenova, “Optical properties of $(\text{Al}_2\text{O}_3)_x(\text{TiO}_2)_{1-x}$ films deposited by the sol–gel method,” *Vacuum*, vol. 76, pp. 219–222, 2004.
- [107] S. B. Rawal, S. Bera, D. Lee, D. Jang, W. I. Lee, “Design of visible-light photocatalysts by coupling of narrow bandgap semiconductors and TiO_2 : effect of their relative energy band positions on the photocatalytic efficiency,” *Catas. Sci. Technol.*, vol. 3, pp. 1822–1830, 2013.
- [108] Y. Xu, M. A. A. Schoonen, “The absolute energy positions of conduction and valence bands of selected semiconducting minerals,” *Am. Mineral.*, vol. 85, pp. 543–556, 2000.
- [109] B. Xin, P. Wang, D. Ding, J. Liu, Z. Ren, H. Fu, “Effect of surface species on Cu- TiO_2 photocatalytic activity,” *Appl. Surf. Sci.*, vol. 254, pp. 2569–2574, 2008.
- [110] S. Permon, G. Berthome, B. Baroux, J. C. Joud, and M. Langlet, “Natural superhydrophilicity of sol–gel derived SiO_2 – TiO_2 composite films,” *J. Mater. Sci.*, vol. 41, pp. 7650–7662, 2006.
- [111] K. Tanabe, T. Sumiyoshi, K. Shibata, T. Kiyoura, J. Kitagawa, “A new hypothesis regarding the surface acidity of binary metal oxides,” *Bull. Chem. Soc. Jpn.*, vol. 47, pp. 1064–1066, 1974.
- [112] A. P. Day, J. D. Oliver, “Changes in membrane fatty acid composition during entry of *Vibrio vulnificus* into the viable but nonculturable state,” *J. Microbiol.*, vol. 42, pp. 69–73, 2004.
- [113] M. M. Or-Rashid, N. E. Odongo, B. W. McBride, “Fatty acid composition of ruminal bacteria and protozoa, with emphasis on conjugated linoleic acid, vaccenic acid, and odd-chain and branched-chain fatty acids,” *J. Anim. Sci.*, vol. 85, pp. 1228–1234, 2007.
- [114] V. Datsyuk, M. Kalyva, K. Papagelis, J. Parthenios, D. Tasis, A. Siokou, I. Kallitsis, C. Galiotis, “Chemical oxidation of multiwalled carbon nanotubes,” *Carbon*, vol. 46, pp. 833–840, 2008.
- [115] J. Diaz, G. Paolicelli, S. Ferrer, F. Comin, “Separation of the sp^3 and sp^2 components in the C1s photoemission spectra of amorphous carbon films,” *Phys. Rev. B*, vol. 54, pp. 8064–8069, 1996.
- [116] S. Beverly, S. Seal, S. Hong, “X-ray photoelectron spectroscopy studies of reactions on chromium metal and chromium oxide surfaces,” *J. Vac. Sci. Technol.*, vol. 18, pp. 1107–1113, 2000.
- [117] J. B. Brzoska, I. B. Azouz, F. Rondelez, “Silanization of solid substrates: A step toward reproducibility,” *Langmuir*, vol. 10, pp. 4367–4373, 1994.
- [118] J. Rathousky, V. Kalousek, M. Kolár, J. Jirkovsky, P. Barták, “A study into the self-cleaning surface properties – The photocatalytic decomposition of oleic acid,” *Catal. Today*, vol. 161, pp. 202–208, 2011.
- [119] J. Zemek, S. Hucek, A. Jablonski, I. S. Tilinin, “Photoelectron escape depth,” *J. Electron Spectrosc. Relat. Phenom.*, vol. 76, pp. 443–447, 1995.
- [120] O. K. Dalrymple, E. Stefanakos, M. A. Trotz, D. Y. Goswami, “A review of the mechanisms and modeling of photocatalytic disinfection,” *Appl. Catal. B-Environ.*, vol. 98, pp. 27–38, 2010.
- [121] J. Kiwi, V. Nadtochenko, “New evidence for TiO_2 photocatalysis during bilayer lipid peroxidation,” *J. Phys. Chem. B*, vol. 108, pp. 17675–17684, 2004.

- [122] O. K. Dalrymple, W. Isaacs, E. Stefanakos, M. A. Trotz, D. Y. Goswami, "Lipid vesicles as model membranes in photocatalytic disinfection studies," *J. Photoch. Photobiol. A*, vol. 211, pp. 64–70, 2011.
- [123] J. Shumann, A. Leichtle, J. Thiery, H. Fuhrmann, "Fatty acid and peptide profiles in plasma membrane and membrane rafts of PUFA supplemented RAW264.7 macrophages," *Plos One*, vol. 6, pp. e24066, 2011.

PUBLICATIONS

CURRICULUM VITAE

Name: Urmas Joost
Date of Birth: 05.11.1985
Nationality: Estonian
Phone number: 5801 7909
E-mail: urmas.joost@ut.ee
Occupation: University of Tartu, Institute of Physics, engineer

Education:
2008 – 2010 University of Tartu M.Sc. (Applied Measurement Science)
2005 – 2008 University of Tartu B.Sc. (Materials Science)
1996 – 2005 Jõhvi High school
1996 Sinimäe High school
1993 – 1996 Toila High school

Language skills: Estonian, English

Career:
2011–2014 University of Tartu, Institute of Physics, Engineer
2010–2011 University of Tartu, Institute of Physics, Specialist
2008–2014 NanoTAK AS
2008– University of Tartu, Institute of Physics, Engineer

List of publications:

Publications included in the thesis:

- U. Joost, K. Juganson, M. Visnapuu, M. Mortimer, A. Kahru, E. Nõmmiste, U. Joost, V. Kisand, A. Ivask, “Antibacterial mechanisms of photocatalytically active anatase nanoparticles based TiO₂ thin films”, Nanotechnology (submitted).
- U. Joost, A. Saarva, M. Visnapuu, E. Nõmmiste, K. Utt, R. Saar, V. Kisand, (2014). Purification of titania nanoparticle thin films: Triviality or a challenge? *Ceramics International*, 40, 7125–7132.
- U. Joost, R. Pärna, M. Lembinen, K. Utt, I. Kink, M. Visnapuu, V. Kisand, V. (2013). Heat treatment and substrate dependent properties of titania thin films with high copper loading. *Physica Status Solidi A – Applications and Materials Science*, 210, 1201–1212.
- R. Pärna, U. Joost, E. Nõmmiste, T. Käämbre, A. Kikas, I. Kuusik, I. Kink, M. Hirsimäki, V. Kisand, (2012). Effect of different annealing temperatures and SiO₂/Si(100) substrate on the properties of nickel containing titania thin sol-gel films", *Physica Status Solidi (a) Volume 209*, 953–965.
- R. Pärna, U. Joost, E. Nõmmiste, T. Käämbre, A. Kikas, I. Kuusik, M. Hirsimäki, I. Kink, V. Kisand, (2011). Effect of cobalt doping and annealing on properties of titania thin films prepared by sol-gel process”, *Applied Surface Science*, 257, 6897–6907.

V. Kisand, U. Joost, V. Reedo, R. Pärna, T. Tätte, J. Shulga, A. Saar, L. Matisen, A. Kikas, I. Kink, (2010). Investigation of nickel doped sol-gel prepared TiO₂ films, *Applied Surface Science*, 256, 4538–4542.

Publications not related to the thesis:

S. Ratso, I. Kruusenberg, M. Vikkisk, U. Joost, E. Shulga, I. Kink, T. Kallio, K. Tammeveski, (2014). Highly active nitrogen-doped few-layer graphene/carbon nanotube composite electrocatalyst for oxygen reduction reaction in alkaline media. *Carbon*, 73, 361–370.

M. Vikkisk, I. Kruusenberg, U. Joost, E. Shulga, I. Kink, K. Tammeveski, (2014). Electrocatalytic oxygen reduction on nitrogen-doped graphene in alkaline media. *Applied Catalysis B: Environmental*, 147, 369–376.

M. Visnapuu, U. Joost, K. Juganson, K. Künnis-Beres, A. Kahru, V. Kisand, A. Ivask, (2013). Dissolution of Silver Nanowires and Nanospheres Dictates Their Toxicity to *Escherichia coli*. *BioMed Research International*, 1–9.

M. Vikkisk, I. Kruusenberg, U. Joost, E. Shulga, K. Tammeveski, (2013). Electrocatalysis of oxygen reduction on nitrogen-containing multi-walled carbon nanotube modified glassy carbon electrodes. *Electrochimica Acta*, 87, 709–716.

E. Itälä, D. T. Ha, K. Kooser, M. A. Huels, E. Rachlew, E. Nõmmiste, U. Joost, E. Kuk, (2011). Molecular fragmentation of pyrimidine derivatives following site-selective carbon core ionisation, *Journal of Electron Spectroscopy and Related Phenomena*, 184, 119–124.

E. Itälä, D.T. Haa, K. Koosera, E. Nõmmiste, U. Joost, E. Kuk, Fragmentation patterns of core ionized uracil, (2011). *International Journal of Mass Spectrometry*, 306, 82–90.

E. Shulga, K. Pohako, A. Treshchalov, U. Joost, V. Kisand, I. Kink, (2011). Functionalisation of aligned carbon nanotubes with nitric acid vapour, *Micro Nano Letters*, 6, 704–708.

Stipends and honours:

2009 University of Tartu, Institute of Physics student stipend

2008 University of Tartu, Institute of Physics student stipend

Hobbies:

Model cars, cycling, reading

ELULOOKIRJELDUS

- Nimi:** Urmas Joost
Sünniaeg: 05.11.1985, Toila vald
Kodakondsus: Eesti
Telefon: 5801 7909
E-post: urmas.joost@ut.ee
Töökoht: Tartu Ülikool, Loodus- ja tehnoloogiateaduskond, Tartu
Ülikooli Füüsika Instituut; insener
- Haridus:**
2008–2010 Tartu Ülikool, Tehnikateaduse magister (rakenduslik mõõteteadus)
2005–2008 Tartu Ülikool, Tehnikateaduse bakalaureus (materjaliteadus)
1996–2005 Jõhvi Gümnaasium
1996 Sinimäe Gümnaasium
1993–1996 Toila Gümnaasium
- Keelteoskus:** Eesti keel, Inglise keel
- Töökogemus:**
2011–2014 Tartu Ülikool, Loodus- ja tehnoloogiateaduskond, Tartu
Ülikooli Füüsika Instituut, Insener
2010–2011 Tartu Ülikool, Loodus- ja tehnoloogiateaduskond, Tartu
Ülikooli Füüsika Instituut, Spetsialist
2008–2014 NanoTAK AS
2008– Tartu Ülikool, Loodus- ja tehnoloogiateaduskond, Tartu
Ülikooli Füüsika Instituut; Insener
- Teaduslik ja arendustegevus:**
Peamised uurimisvaldkonnad:
Metallidega dopeeritud titaan dioksiid kilede valmistamine sool-geel meetodil ja nende karakteriseerimine erinevate meetoditega (röntgen fotoelektron spektroskoopia, Raman spektroskoopia, UV-Vis spektroskoopia, teravik-mikroskoopia, aatomjõumikroskoopia, sünkrotron-röntgenspektroskoopia).
- Publikatsioonide loetelu:**
Publikatsioonid doktoritöös:
U. Joost, K. Juganson, M. Visnapuu, M. Mortimer, A. Kahru, E. Nõmmiste, U. Joost, V. Kisand, A. Ivask, “Antibacterial mechanisms of photocatalytically active anatase nanoparticles based TiO₂ thin films”, Nanotechnology (submitted).
U. Joost, A. Saarva, M. Visnapuu, E. Nõmmiste, K. Utt, R. Saar, V. Kisand, (2014). Purification of titania nanoparticle thin films: Triviality or a challenge? *Ceramics International*, 40, 7125–7132.
U. Joost, R. Pärna, M. Lembinen, K. Utt, I. Kink, M. Visnapuu, V. Kisand, V. (2013). Heat treatment and substrate dependent properties of titania thin films with high copper loading. *Physica Status Solidi A – Applications and Materials Science*, 210, 1201–1212.

- R. Pärna, U. Joost, E. Nõmmiste, T. Käämbre, A. Kikas, I. Kuusik, I. Kink, M. Hirsimäki, V. Kisand, (2012). Effect of different annealing temperatures and SiO₂/Si(100) substrate on the properties of nickel containing titania thin sol-gel films, *Physica Status Solidi (a)* Volume 209, 953–965.
- R. Pärna, U. Joost, E. Nõmmiste, T. Käämbre, A. Kikas, I. Kuusik, M. Hirsimäki, I. Kink, V. Kisand, (2011). Effect of cobalt doping and annealing on properties of titania thin films prepared by sol-gel process”, *Applied Surface Science*, 257, 6897–6907.
- V. Kisand, U. Joost, V. Reedo, R. Pärna, T. Tätte, J. Shulga, A. Saar, L. Matisen, A. Kikas, I. Kink, (2010). Investigation of nickel doped sol-gel prepared TiO₂ films, *Applied Surface Science*, 256, 4538–4542.

Publikatsioonid, mis ei ole doktoritööga seotud:

- S. Ratso, I. Kruusenberg, M. Vikkisk, U. Joost, E. Shulga, I. Kink, T. Kallio, K. Tammeveski, (2014). Highly active nitrogen-doped few-layer graphene/carbon nanotube composite electrocatalyst for oxygen reduction reaction in alkaline media. *Carbon*, 73, 361–370.
- M. Vikkisk, I. Kruusenberg, U. Joost, E. Shulga, I. Kink, K. Tammeveski, (2014). Electrocatalytic oxygen reduction on nitrogen-doped graphene in alkaline media. *Applied Catalysis B: Environmental*, 147, 369–376.
- M. Visnapuu, U. Joost, K. Juganson, K. Künnis-Beres, A. Kahru, V. Kisand, A. Ivask, (2013). Dissolution of Silver Nanowires and Nanospheres Dictates Their Toxicity to *Escherichia coli*. *BioMed Research International*, 1–9.
- M. Vikkisk, I. Kruusenberg, U. Joost, E. Shulga, K. Tammeveski, (2013). Electrocatalysis of oxygen reduction on nitrogen-containing multi-walled carbon nanotube modified glassy carbon electrodes. *Electrochimica Acta*, 87, 709–716.
- E. Itälä, D. T. Ha, K. Kooser, M. A. Huels, E. Rachlew, E. Nõmmiste, U. Joost, E. Kuk, (2011). Molecular fragmentation of pyrimidine derivatives following site-selective carbon core ionisation, *Journal of Electron Spectroscopy and Related Phenomena*, 184, 119-124.
- E. Itälä, D.T. Haa, K. Koosera, E. Nõmmiste, U. Joost, E. Kuk, Fragmentation patterns of core ionized uracil, (2011). *International Journal of Mass Spectrometry*, 306, 82–90.
- E. Shulga, K. Pohako, A. Treshchalov, U. Joost, V. Kisand, I. Kink, (2011). Functionalisation of aligned carbon nanotubes with nitric acid vapour, *Micro Nano Letters*, 6, 704–708.

Saadud uurimistoetused ja stipendiumid:

2009 Tartu Ülikooli Füüsika Instituudi üliõpilasstipendium

2008 Tartu Ülikooli Füüsika Instituudi üliõpilasstipendium

Huvialad:

Automudelism, jalgrattasõit, ilukirjandus.

DISSERTATIONES SCIENTIAE MATERIALIS UNIVERSITATIS TARTUENSIS

1. **Martin Järvekülg.** Tubular microstructures by Hf-, Zr- and Ti-butoxide gel sheet rolling. Tartu, 2011, 112 p.
2. **Sergei Vlassov.** Investigation of nanoscale interactions and mechanical properties of nanostructures using quartz tuning fork based real-time measurements. Tartu, 2011, 171 p.
3. **Margus Kodu.** Pulsed Laser Deposition of Magnesium Oxide and Barium Ternary Oxides for Plasma Display Protective Layers. Tartu, 2011, 89 p.
4. **Rainer Pärna.** Surface studies of some oxide films. Tartu, 2011, 129 p.
5. **Jevgeni Šulga.** Self-assembly and interaction of nanostructures. Tartu, 2011, 114 p.
6. **Wojciech Kuznik.** Quantum-chemical computer simulations of the linear and non-linear optical properties of pyrazoloquinoline and dicyanopyrazine derivatives. Tartu, 2012, 89 p.
7. **Leonid Dorogin.** Structural and tribological properties of zero- and one-dimensional nanocrystals. Tartu, 2012, 193 p.
8. **Viljar Palmre.** Fabrication and characterization of microporous carbon-based electroactive polymer actuators. Tartu, 2012, 99 p.
9. **Madis Paalo.** Synthesis of CNT-metal oxide nanocomposites: sol-gel process, rheology, structural and functional properties. Tartu, 2014, 175 p.
10. **Raul Välbe.** Development of ionic liquid composites by sol-gel method for elaboration of industrial nano- and microstructures. Tartu, 2014, 97 p.